Quantification of Dynamic Changes of Hemodynamic and Metabolic Responses to Brachial Artery Occlusion: A Broadband Near-Infrared Spectroscopy Study

by

Caroline Carter

THESIS

Presented to the Faculty of the Graduate School of

The University of Texas at Arlington in Partial Fulfillment

of the Requirements

For the Degree of

MASTER OF SCIENCE IN BIOMEDICAL ENGINEERING

THE UNIVERSITY OF TEXAS AT ARLINGTON

DECEMBER 2023

Acknowledgements

I am deeply indebted to Dr. Hanli Liu, whose unwavering support and mentorship have been instrumental in shaping my academic journey throughout my undergraduate and master's degree. Her wealth of knowledge, invaluable advice, and steadfast support have made an immeasurable impact on my educational pursuits, spanning both my undergraduate and master's studies, and the arduous process of crafting this thesis.

My sincere appreciation extends to my esteemed defense committee members, Dr. Brothers and Dr. Alexandrakis. I would like to offer special thanks to Dr. Brothers for his invaluable guidance and the exceptional contributions of his recruitment team. Furthermore, I would like to express my profound gratitude to all my past and present lab colleagues over the years. Their unwavering support and collaborative spirit have played a pivotal role in my academic endeavors. I extend my heartfelt thanks to Dr. Sadra Shahdadian, Haylea Renguul, and John Kolade for their invaluable assistance in the analysis of bbNIRS and FMD data. I would also like to acknowledge the contributions of Claire Sissons, Fiza Saeed, and Binita Kc whose assistance has been instrumental in shaping my thesis. Special mention goes to Dr. Sadra Shahdadian for imparting a wealth of knowledge on diverse data processing and analysis techniques.

Finally, I extend my gratitude to my friends and family, whose love and support have been a constant source of inspiration throughout my academic odyssey. My deepest appreciation goes to my parents for their belief in me and always supporting my wildest dreams.

Table of Contents

List of figures

Abstract

Measuring Endothelial Dysfunction with Wavelet Transform Coherence for Analysis of Hemodynamic-Metabolic Activity During Brachial Artery Occlusion.

Caroline Carter

The University of Texas at Arlington, 2023

Supervising Professor: Dr. Hanli Liu

Cardiovascular disease (CVD) is a leading cause of death in the United States, and non-Hispanic African Americans are at higher risk than other racial and ethnic groups. Endothelial dysfunction is a major contributor to CVD development and progression. Remote ischemic pre/conditioning (RIC), which involves exposing cells or tissues to brief sublethal stress, has been shown to protect cardiovascular cells from ischemia and reperfusion injury, including CVD. This study aimed to investigate hemodynamic and metabolic dynamics in response to 5-min forearm arterial occlusion using broadband near-infrared spectroscopy. My thesis is a tripartite investigation that weaves RIC, mitochondrial dynamics, and health disparities together. Specifically, 17 The participants were instructed to lay down and follow a brachial artery occlusion protocol in the upper arm. A broadband spectrometer was then placed on the brachioradialis muscle below the cuff, proximal to the wrist. The measurement protocol consisted of a 5-min rest, 5-min arm cuff under 220 torr, and 3-min recovery. After the data processing, several key results were obtained. (1) Dynamic alterations in oxygenated and deoxygenated hemoglobin (D[HbO] and D[HHb]) showed well-known, expected patterns in response to a 5-min RIC. (2) Dynamic alterations of

oxidized cytochrome c oxidase ([CCO]) exhibited a rapid increase, followed by a stationary amplitude across the 5-min RIC. (3) The wavelet transform coherence analysis enabled us to determine vascular and mitochondrial coupling and demonstrated decoupling and recoupling phases during the occlusion and recovery periods. Finally, (4) possible disparities in hemodynamic and metabolic dynamics and their coupling exist during and after the occlusion, revealing the nuanced differences between African American and Caucasian populations.

CHAPTER 1

1 Introduction

Cardiovascular disease (CVD) is a formidable global health challenge affecting nearly one-third of the adult population [1, 2, 3]. A striking racial disparity exists, with African Americans (AA) and Caucasians (WH) exhibiting distinct prevalence rates. Endothelial dysfunction (ED), a pivotal early indicator of CVD, involves an imbalance in vascular homeostasis characterized by reduced vasodilator bioavailability and increased vasoconstrictors, particularly nitric oxide (NO) [3, 4]. This dysfunction, linked to oxidative stress, is more prevalent in AA compared to WH individuals [4, 5, 6]. The intricate interplay of genetic, environmental, physiological, and socioeconomic factors contributes to this racial disparity [6, 7, 8, 9]. Given the earlier onset, increased severity, and poorer outcomes of CVD in AA populations, understanding the physiological mechanisms, particularly related to endothelial function, is essential for developing targeted therapeutic interventions and addressing racial disparities in CVD outcomes [10, 11, 12].

1.1 Forearm Arterial Occlusion

Using acute Forearm Arterial Occlusion (FAO) emerges as a noninvasive therapeutic strategy capitalizing on the body's inherent protective capabilities against ischemia-reperfusion injury [13, 14, 15,]. This phenomenon induces brief non-lethal ischemia-reperfusion episodes in one part of the body, conferring resistance to subsequent episodes in a remote organ or tissue [16, 17, 18]. When repeated, FAO has potential in reducing the impact of ischemic heart diseases and improving cardiovascular outcomes [14, 19, 21, 22]. Beyond heart protection, FAO extends to inter-organ protection against ischemia-reperfusion injury, influencing mitochondrial dynamics and function.

[22, 23]. As we delve into the physiological mechanisms of FAO, particularly its impact on mitochondrial function, we recognize the potential implications for addressing cardiovascular health disparities. Mitochondrial function is increasingly linked to CVD health disparities, offering a promising avenue for preventive and therapeutic strategies [19, 23, 24]. The ongoing investigation of FAO's protective mechanisms and its systemic effects on various organs, including the heart and brain, opens new possibilities for therapeutic interventions [25, 26]. Our study aims to contribute to the understanding of how mitochondria are involved in the context of FAO, holding promise for advancing CVD prevention and novel detection strategies.

1.2 Tools for Noninvasive detection

Broadband Near-Infrared Spectroscopy (bbNIRS) is a pivotal tool in this study, noninvasively monitoring both hemodynamic and metabolic functions [26, 27, 28, 29]. Complementing this, the study employs Flow-Mediated Dilation (FMD), a non-invasive Doppler ultrasound technique that measures the dilation response of an artery to increased blood flow, crucial for evaluating endothelial function and detecting vessel dilation [11, 31]. However, during the dynamic period of forearm occlusion, traditional Doppler ultrasound does not capture video data. This limitation is addressed by the innovative use of bbNIRS, which not only complements FMD by providing data on hemodynamics and mitochondrial activity, but also captures endothelial activity within the infra-slow oscillations (ISO) frequency bands during occlusion [28, 29]. This multi-dimensional approach enhances our understanding of the complex physiological responses in AA and WH populations. It sheds light on potential mechanisms contributing to CVD disparities and offers novel avenues for therapeutic intervention.

1.3 Hemodynamic and Metabolic Chromophore Detection

The focus of our study is to assess the coherence between oxygenated hemoglobin (HbO) and cytochrome C oxidase (CCO) signals in the forearm of healthy adults, specifically from AA and WH populations, in the context of ISO frequency bands. ISO, representing vascular rhythms, offers insights into endothelial, neurogenic, and myogenic activities [28, 29, 30]. By exploring variations in vascular responses within these populations, we aim to quantify differences in the predisposition to CVD. The amplitude of HbO and CCO signals within the ISO bands provides additional insights into the forearm's capacity to respond to hemodynamic and metabolic demands related to cardiovascular health [28, 29, 30, 31]. CCO is an indicator of ATP production and metabolic function and can be detected using bbNIRS [29, 30]. This non-invasive detection of CCO is of notable distinction, as it has not previously been investigated during ischemic occlusion as an indicator of mitochondrial health. [28, 29, 32]. Quantification of HbO, deoxyhemoglobin (HHb), Total Hemoglobin blood flow (HbT), hemoglobin differences (HbD), and CCO are as delineated in the cited publication [28, 29, 32]

1.4 Wavelet Transform Coherence

The Wavelet Transform Coherence (WTC) technique is a powerful tool that provides a unique perspective on the hemodynamic-metabolic coupling during cuff occlusion [33, 34]. This technique allows for the visualization of ISO bands, offering insights into the complex interplay between hemodynamic and metabolic processes [28, 29, 30]. By generating an overcomplete representation of a time-domain signal, WTC enables a detailed examination of the coherence between HbO and CCO signals across various frequencies at each time point [34, 35, 36]. This approach not only enhances our understanding of the physiological responses during cuff

occlusion but also opens new avenues for investigating the underlying mechanisms of cardiovascular disease disparities. The introduction of WTC in this study marks a significant advancement in the non-invasive assessment of endothelial function and health.

1.5 Study Goals

This paper articulates a tripartite investigation, weaving together FAO, mitochondrial dynamics, and health disparities. The three primary goals of this study are outlined as follows:

(1) Dynamic Alterations Under FAO: To investigate dynamic alterations of oxygenated hemoglobin ([HbO]) and oxidized cytochrome c oxidase ([CCO]) under 5-minute FAO by forearm arterial occlusion, which are measured with broadband near-infrared spectroscopy (bbNIRS).

(2) Physiological Coupling Analysis: Quantifying the physiological coupling or interaction between hemodynamic and metabolic activity before, during, and after 5-minute FAO using wavelet transform coherence (WTC) analysis.

(3) Disparity Examination: Observing and examining possible disparities in the dynamic indices of hemodynamic-metabolic coupling during and after 5-minute FAO, with a particular focus on unraveling the nuanced differences between AA and WH populations.

This study, positioned at the intersection of cutting-edge cardiovascular research and the imperative to address health disparities, holds promise for unveiling new therapeutic avenues and public health initiatives to address the pressing concern of cardiovascular health disparities.

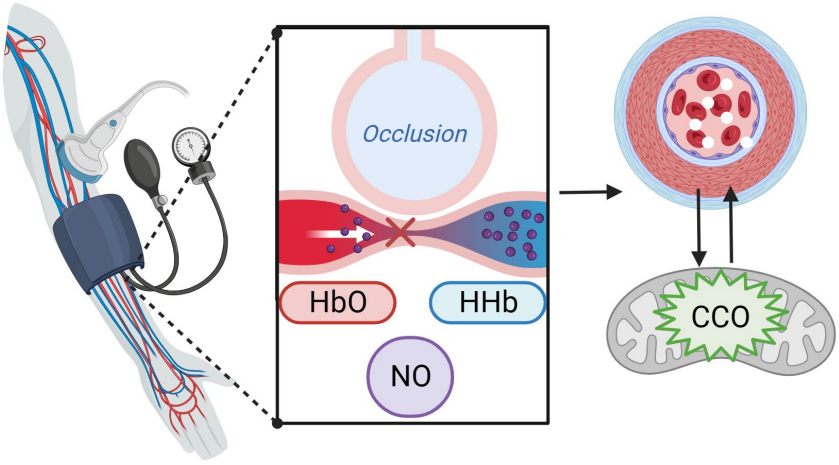

Figure 1. Anatomical Illustration of the Human Right Forearm and Cardiovascular System: A Schematic depiction of FAO.

Figure 1 provides an anatomical illustration of the human right forearm, featuring the cardiovascular system. Positioned on the forearm is an inflatable arm cuff, located distal to the elbow, designed to occlude venous blood flow. Additionally, an ultrasound probe is depicted on the upper forearm, aimed at imaging the brachial artery. The illustration includes a representation of the occlusion event on a capillary, where the venous blood inflow is halted by the occlusion air puff cuff. This event triggers gas exchange into deoxygenated blood on the opposite side of the vein, releasing molecules such as nitric oxide labeled (NO) in purple, and inducing shear stress on the vessel. The schematic illustrates oxygenated blood labeled as HbO in red and deoxygenated blood labeled as HHb in blue.

The occlusion event initiates a cascade of beneficial molecules released into the bloodstream [14, 16, 18]. As the supply and demand of blood flow to muscle cells decrease during occlusion, muscle cells produce higher amounts of ATP within the mitochondria [19, 23, 24]. This noninvasively monitored response involves observing the change in oxiCCO, depicted in green. The mitochondrial response acts as a catalyst for vessel contraction. During FAO, this continuous

training of both hemodynamic and metabolic functions can flow through the bloodstream, potentially benefiting a diseased heart, as illustrated in the figure depicting an injured heart. Over time, these beneficial molecules may contribute to repairing minor cardiac damage. Furthermore, these molecules can traverse the blood-brain barrier, theoretically aiding in reversing the effects of stroke in the brain.

1.6 Ethics

Ethical approval was obtained from the University of Texas at Arlington Institutional Review Board (#2020-0054). All participants were informed of the experimental procedures and risks before participating. Verbal and written informed consent were obtained from each participant. The experimental protocols aligned with the guidelines set forth by the Declaration of Helsinki except for registration in a database.

Chapter 2

2 Methodology

2.1 Participant Demographic

Our study comprised of self-identifying African American and non-Hispanic Caucasian individuals, who reported both biological parents are also of same race, reflective of the diverse population within the Dallas-Fort Worth Metroplex, Texas, USA. A total of 17 healthy participants were recruited from February 2023 to November 2023 through a combination of flyers, social media, and word-of-mouth referrals. The inclusion criteria specified participants of either Black or White race/ethnicity, with an age range of 18 to 35 years and a body mass index (BMI) falling between 18.5 and 29.9 kg/m². The cohort consisted of 7 Black participants (20±2 years) and 5 White participants (25±7 years), with equal representation of both genders, including 4 men and 13 women [37, 38, 39].

2.2 Exclusion Criteria and Eligibility Assessment

Eligibility for participation was meticulously determined by the kinesiology lab based on a comprehensive set of criteria. Self-reported racial identity played a pivotal role in confirming eligibility. Exclusion criteria encompassed individuals who were tobacco users and competitive athletes. In addition, prospective participants were required to be free from overt cardiovascular, metabolic, and neurological diseases, while refraining from the use of vasoactive prescription medications or supplements. [37,38,39]

Participants with a history of various microvasculature diseases, such as Reynaud's disease, cold-induced urticaria, cryoglobulinemia, among others, were also ineligible. Furthermore, individuals currently taking prescription medications and those with a body mass index exceeding 30 kg/m² were excluded from the study. Given the impact of smoking on peripheral vasculature, both current smokers and individuals who had engaged in regular smoking (>1 pack per two weeks) within the previous two years were not considered eligible for participation [39.40].

2.3 Experimental Protocol

A The research methodology employed here closely follows that of a study conducted by Shahdadian et al. in 2022. The experimental setup utilized a 2-channel system comprising two branches of a broadband white light source (Model 3900e, Illumination Technologies, NY, USA) and two CCD array spectrometers (QEPRO, Ocean Optics Inc., Orlando, FL, USA) serving as light detectors [28,29,32]. In each channel, one fiber bundle was dedicated to deeper light delivery to the forearm, while another facilitated shallower light delivery, maintaining a source-detector separation of 1 cm for the shallow layer and 3 cm for the deeper layer.

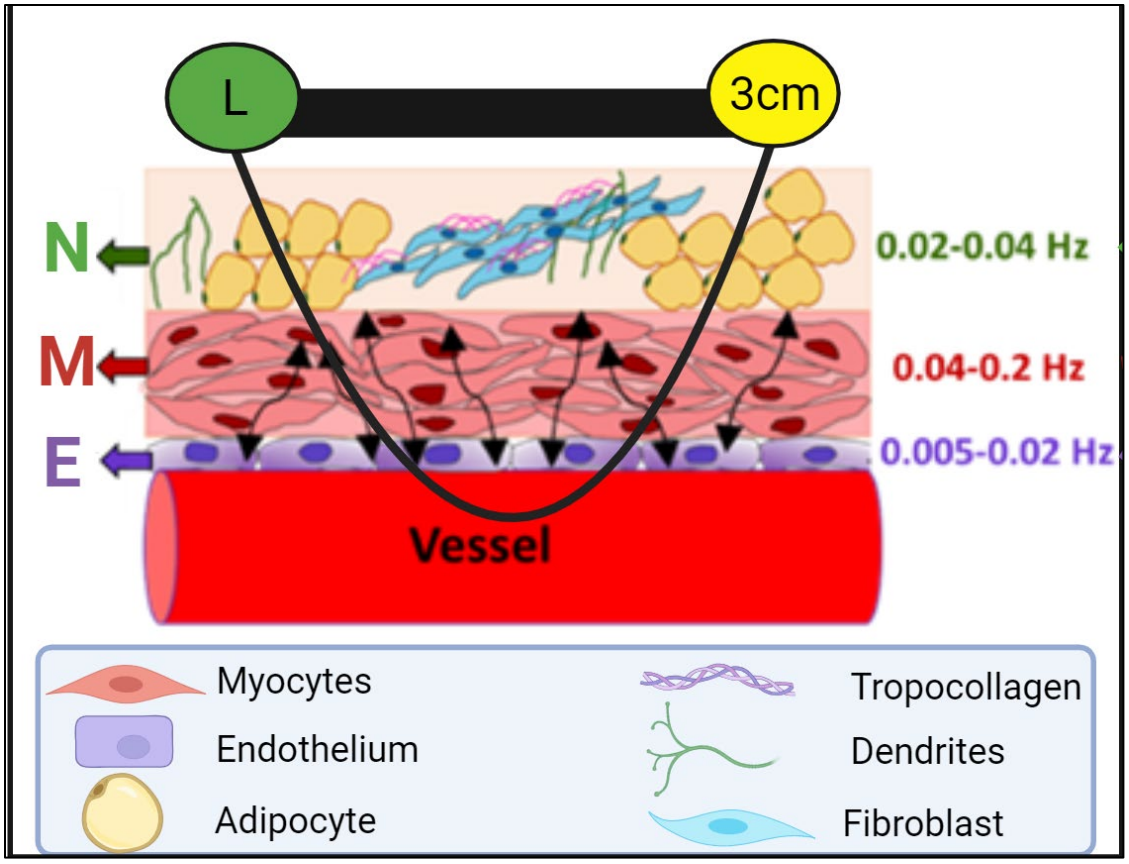

Figure 2. Illustration of the bbNIRS probe on the forearm physiological tissue with frequency bands.

In figure 2. The diagram shows an illustrative example of the 3cm distance deep penetration using the bbNIRS system. This illustration shows how light penetrates through multiple frequency bands to the microcapillaries vessels. That the green circle with the L label is an indication of the light source the black rectangle strip connected to the light source is indication of the 3D printed ninja flex band. The yellow 3-centimeter circle is an indication of the QE pro detector which is placed 3cm away from the light source. To secure optimal contact with the forearm and accommodate individual variations in forearm curvature, a custom-designed 2-channel probe holder was created [28,29,32]. This holder, crafted using 3D printing technology and a flexible material, ensured both comfortable and secure attachment of the fiber bundles to the forearm skin. The probe holder was

affixed to each participant's forearm using hook-and-loop fasteners, with additional adhesive medical tape applied at the probe-skin interface. This dual fastening approach aimed to enhance the stability of the probe on the forearm, minimizing motion artifacts without excessive tightening of the fasteners. The green N stands for the neurogenic frequency band which corresponds to the layer of tissue that includes dendrites adipocytes fibroblasts and other topo collagen material which is found at 0.02-0.04 Hertz. The red M is an indication of the myogenic frequency band which includes myocytes, which is commonly found at 0.04-0.2 Hertz. The purple E is an indication of the endothelial frequency band which makes up the endothelium or lining of the blood vessel which is commonly found at 0.005-0.02 Hertz. The vessel is indicated by the red cylinder in the context of this study our vessels are capillaries and micro vessel structures within the forearm, [28,29,32].

During the setup for the experiment, subjects laid down and relaxed their arm before an automatic arm cuff was placed on their forearm, just past their elbow, and a doppler ultrasound images the brachial artery on the upper arm. Then, an OceanOptics bbNIRS spectrometer was placed on the brachioradialis muscle below the cuff proximal to the wrist and strapped securely. Participants underwent FMD protocol, the researchers monitored baseline, where the subject remained at rest for 5 minutes. Followed by 5 minutes of arm cuff inflation to 220 torr, during which only bbNIRS data was collected. Then 3 minutes of recovery from the start of cuff release to allow blood flow recovery [37,38,39,40].

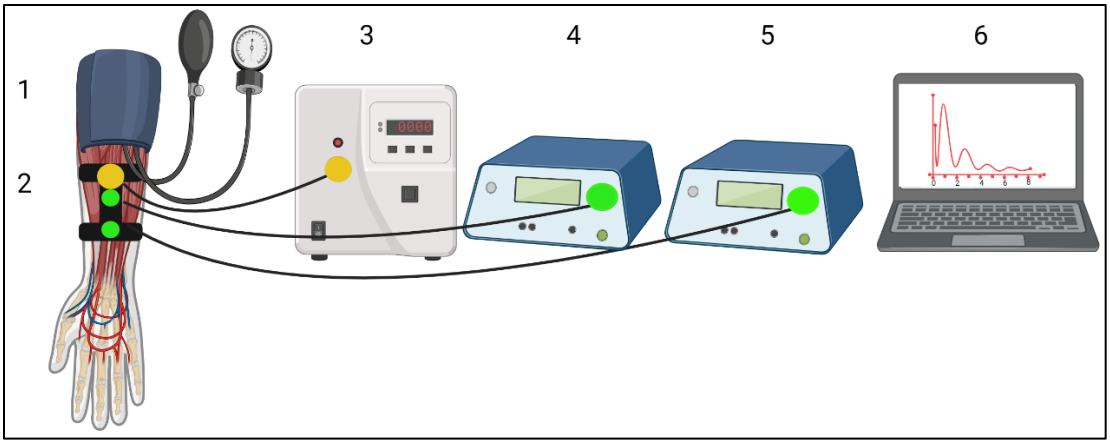

Figure 3. Illustration of the bbNIRS arm band and equipment set up.

Figure 3.1 illustrates the setup for Flow-Mediated Dilation (FMD). An inflatable arm cuff, pressurized to 220 mmHg, is positioned below the elbow. Figure 3.2 depicts the placement of the broadband Near-Infrared Spectroscopy (bbNIRS) probe on the lower forearm muscles, specifically away from wrist veins. In Figure 3.3, a broadband light source is shown as part of the experimental setup. Figures 3.4 and 3.5 showcase the 1cm and 3cm QE-Pro detectors, respectively. Further details can be found in the appendix. Figure 3.6 illustrates the data collection process using Oceanview software on a computer.

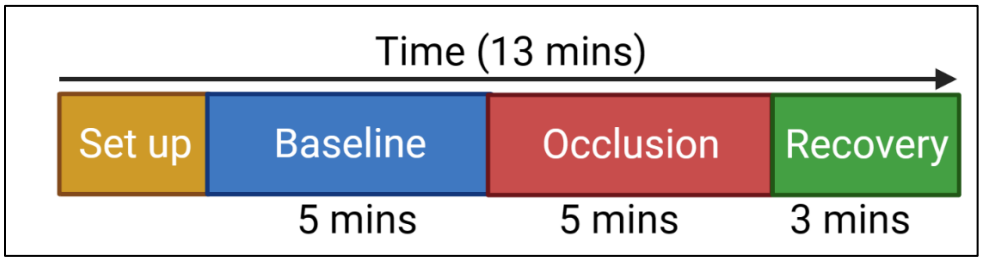

Figure 4. Experimental Protocol Timeline over 13 minutes

Figure 4 provides an overview of the experimental protocol. The yellow section denotes the initial setup, followed by a 5-minute baseline data collection phase in blue. The red segment represents the 5-minute cuff occlusion period, and the subsequent green section signifies the 3-

minute recovery data collection. In total, the experimental protocol spans 13 minutes, encompassing setup, baseline, occlusion, and recovery phases.

2.4 Flow Mediated Dilation Protocol

Peripheral vascular function was assessed using FMD, as previously described (12,36,39). Briefly, a pneumatic cuff connected to a rapid inflation device (Hokanson Model E20 Rapid Cuff Inflator; Bellvue, WA) was placed just distal to the antecubital fossa and the brachial artery was imaged using high-resolution, duplex Doppler ultrasound [39]. An adjustable frequency (10–13 MHz) linear array transducer (LOGIQ P5, GE Healthcare; Chicago, IL) was selected for optimal B-mode signals of the brachial artery and held in a stereotactic clamp 5–10 cm proximal to the antecubital fossa. Once a suitable image was obtained and optimized for clear delineation between the lumen and vessel walls, duplex mode (at a pulsed frequency of 5 MHz) was utilized for the continuous measurement of brachial artery diameter and blood velocity[39]. The sample volume was set to encompass the entire lumen, without extending into the surrounding tissue, at an insonation angle of 60°. All images were recorded using a commercially available screen capture software (Elgato Video Capture, Corsair; Fremont, CA) [12,36,39]. Each image was analyzed offline using continuous edge-detection software (Cardiovascular Suite, Quipu; Pisa, ITA) along a section of the artery with clearly defined vessel walls, while second-by-second blood velocity was taken as the entire Doppler envelope. Following instrumentation and a 15 min stabilization period FMD was assessed. After a 5 min baseline, during which brachial artery diameter and blood velocity were continuously measured, the pneumatic cuff was inflated to ~220 mmHg for 5 min to elicit ischemia. Upon cuff deflation, brachial artery diameter and blood velocity were recorded for an additional 3 min.

2.5 Quantification of Δ[HbO], Δ[HHb], Δ[HbT], and Δ[oxCCO] time series.

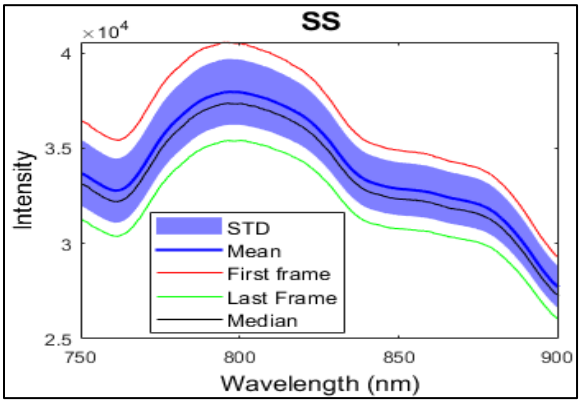

Figure 5. Averaged Raw Optical Spectra.

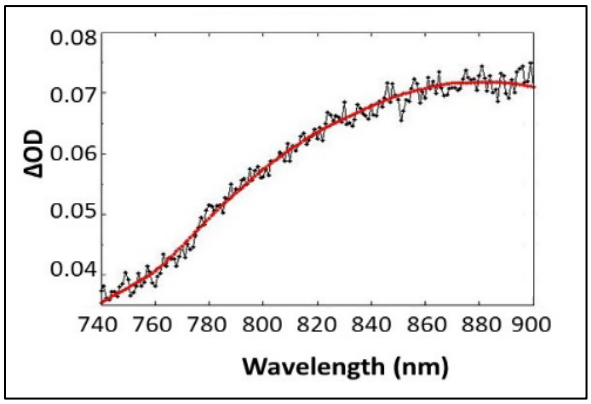

Figure 6. Conversion to Optical Density for each Wavelength (nm).

Figure 5 presents a collection of raw optical spectra obtained through broadband Near-Infrared Spectroscopy (bbNIRS). The spectra, acquired over a 7-minute data collection period, are depicted with shading to represent the mean and median values. The standard deviation is illustrated, and the highest and lowest spectra are outlined, providing a comprehensive view of the spectral variability during the measurement duration. Figure 6 shows the change in optical density over wavelengths (nm) from 740-900nm. A line of best fit is shown in red to notate the curvature of the change in optical density. Differential path length factor (DPF) of a wavelength can be

calculated using the equation in figure 7 using μa which is spectral amplitude, and μs which is spectral scattering values of a certain medium. The medium used in our study is the forearm which has designated μa and μs values used in previous literature [21,27]

$$DPF(\lambda) = \frac{\sqrt{3\mu_s'(\lambda)}}{2\sqrt{\mu_a(\lambda)}} * \frac{r\sqrt{3\mu_a(\lambda)\mu_s'(\lambda)}}{r\sqrt{3\mu_a(\lambda)\mu_s'(\lambda)}+1}$$

Figure 7. Differential Path Length Factor equation.

Broadband Near-Infrared Spectroscopy (bbNIRS) has been a subject of investigation for over two decades [28,29,32], recognized as a reliable tool for quantifying cortical changes in Δ[HbO], Δ[HHb], and Δ[CCO] using the modified Beer–Lambert law (MBL). In our study, we adhered to established protocols, focusing on the spectral range of 780–900 nm [27, 28, 32]. Employing MBL and multiple linear regression analysis with a low-pass filter at 0.2 Hz [28,29], we quantified prefrontal Δ[HbO] and Δ[CCO]. Detailed derivations and steps are available in Refs. [7,28,29,32]. This approach provided a time series of Δ[HbO] and Δ[CCO] for the 13-minute protocol at a sampling frequency of 0.67 Hz, ensuring accurate chromophore concentration estimation with minimal error propagated from noise [32,33,34,35].

Simultaneously, we employed a non-linear, curve-fitting regression algorithm inspired by Wang et al. [32] to quantify changes in chromophore concentrations induced by forearm occlusion. This process included creating an extinction coefficient matrix for forearm tissues based on wavelengths emitted by the bbNIRS device. Subsequent data processing in MATLAB followed established methodologies by Wang et al. [32], incorporating the construction of an extinction coefficient matrix specific to forearm tissues and applying multiple linear regression analysis to identify optimal fits for Δ[HbO], Δ[HHb], and Δ[CCO]. These robust analyses ensured a comprehensive assessment of chromophore changes in the forearm,

integrating established methodologies from prior studies in the field.

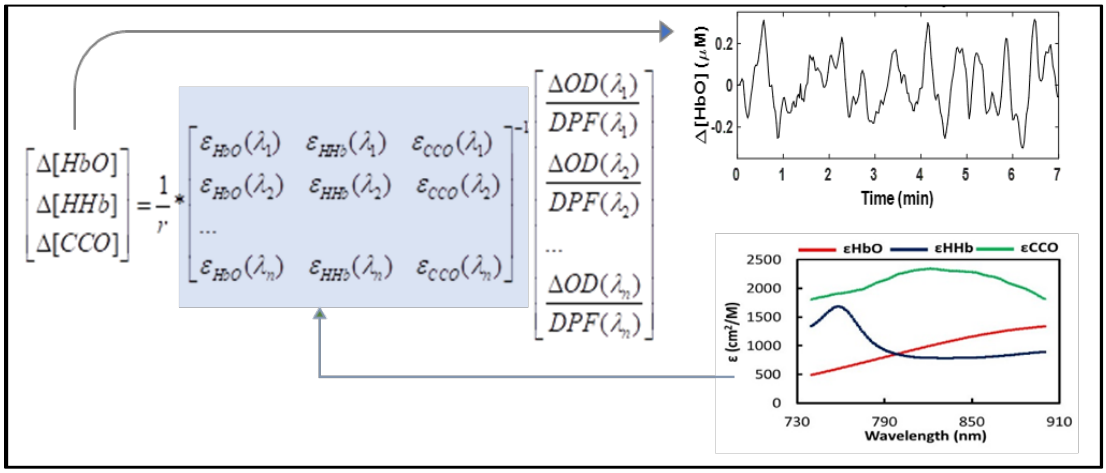

Figure 8. Quantification of temporal Δ [HbO] and Δ [CCO].

Figure 8 illustrates the three-step algorithm employed for the quantification of time-dependent changes in Δ[HbO], Δ[HHb], and Δ[CCO]. The matrix solution process is depicted on the left within the blue box, involving the pseudo inversion of the $n \times 3$ ε matrix at each time point, as detailed in the lower right box. Subsequently, the resulting Δ[HbO], Δ[HHb], and Δ[CCO] concentrations are graphed to demonstrate the concentration changes over time (mins), as presented in the top right box [27,28,29,32].

2.6 Wavelet Transform Coherence Algorithm

In addition to this methodology, the study incorporated the Wavelet Transform Coherence (WTC) technique. The WTC method is used to generate an overcomplete representation of a time-domain signal. A Morlet wavelet, a Gaussian-windowed sinusoidal function, was adopted for the CWT computations, as it aligns with the methodology [29,32,42]. The Gaussian nature of the Morlet

wavelet plays a crucial role in the convolution process during the Fourier transform, preserving both time and frequency information. Subsequently, the CWT process was applied to both the HbO and CCO signals. The cross-correlation between these two signals was then computed, resulting in a coherence value across various frequencies at each time point. To visualize the coherence, these values were presented using a color bar that ranges from blue to red, with red indicating the highest coherency in the plot. Additionally, black contour lines encircled regions of significant coherence within the heat map. Black arrows were incorporated within these significant areas to denote the phase difference between the two input signals. Specifically, a right-pointing arrow symbolizes a 0-degree difference, signifying that the signals are entirely in-phase. Likewise, an upward-pointing arrow signifies a 90-degree difference where HbO leads CCO, a leftward direction denotes a 180-degree difference (representing anti-phase behavior) where CCO leads HbO, and a downward arrow signifies a 270-degree difference. Finally, the shaded region at the periphery of the heat maps corresponds to the Cone of Interference (COI). This inclusion is due to the tapered nature of the Morlet wavelet, which necessitates the addition of zero-padding to each signal before convolution to ensure the first time-series point is included during the Fourier Transform. As a result, the data at the edges of the continuously wavelet-transformed signals are not genuine convolution results and are therefore indicated as points within the COI, not factored into the analysis of the WTC heat maps.

Chapter 3

3 Results

The results section presents dynamic temporal curves for Δ[HbO], Δ[HHb], Δ[CCO], and Δ[HbT] during the baseline, followed by WTC graphs illustrating the occlusion period, with data segregated for racial disparity analysis. The FMD results were analyzed during the recovery phase but were excluded due to time constraints.

3.1 Dynamic Temporal Time Curves

Dynamic changes in Δ[HbO], Δ[HHb] and Δ[HbT] under 5-min forearm arterial cuff

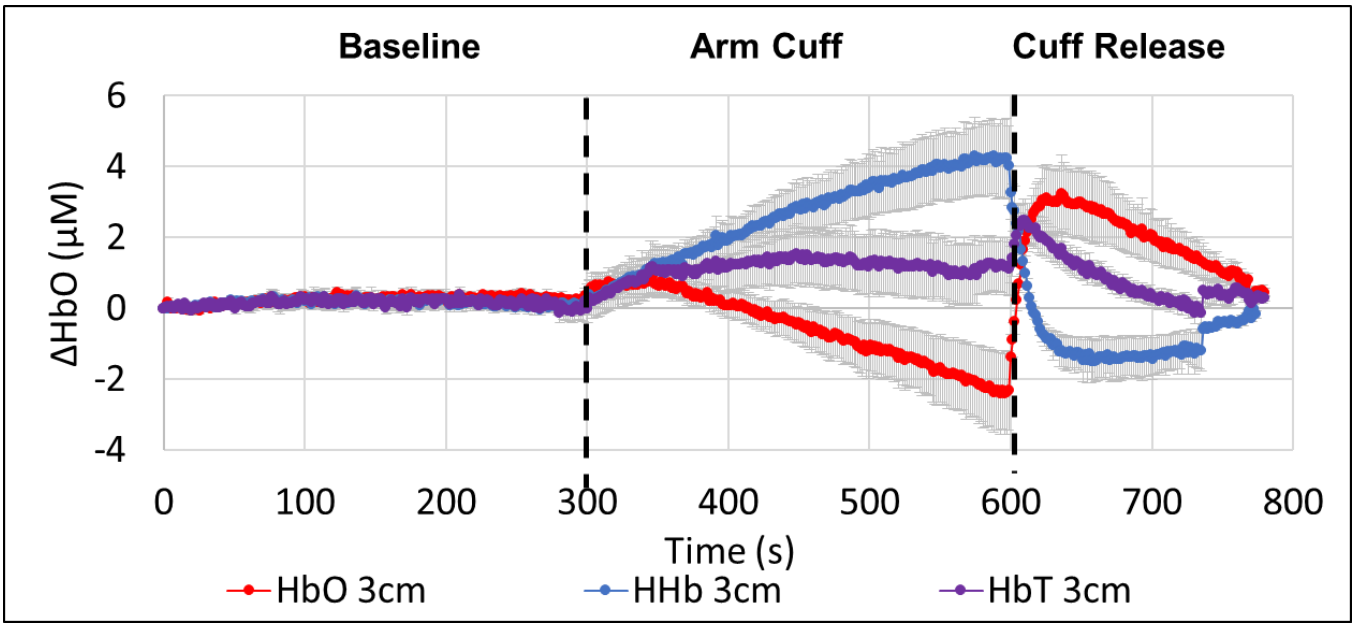

Figure 9. Dynamic changes in Δ [HbO], Δ [HHb], and Δ [HbT] under 5-min forearm arterial cuff.

Figure 9 illustrates the dynamic alterations in oxygenated hemoglobin (Δ[HbO]), deoxygenated hemoglobin (Δ[HHb]), and total hemoglobin concentration (Δ[HbT] = Δ[HbO] + Δ[HHb]) throughout a 5-minute forearm arterial occlusion. The graph is segmented into three distinct time

intervals: baseline (0s-300s), arm cuff application (300s-600s), and cuff release (600s-780s), spanning a total duration of 13 minutes. The x-axis represents time in seconds, while the y-axis depicts the change in HbO concentration in micromolar (μM), ranging from -4 to 6 μM. The observed results align with anticipated trends established in previous publications, demonstrating a gradual decrease in Δ[HbO] indicated by the red line, an increase in Δ[HHb] represented by the blue line, and a relatively constant Δ[HbT] denoted by the purple line during the cuff application. Following the initial cuff release, there is a rapid return of the parameters to baseline levels during the 3-minute recovery period.

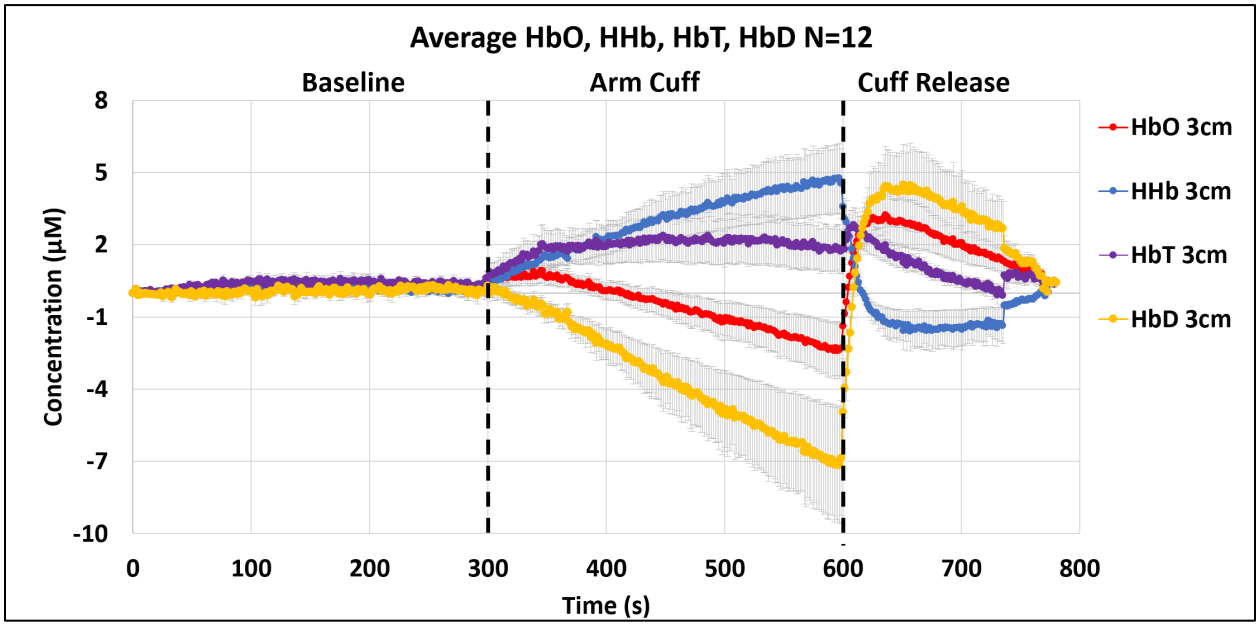

Figure 10. Dynamic changes in Δ[HbO], Δ[HHb], Δ[HbT], and Δ[HbD] under 5-min forearm arterial cuff.

Figure 10 illustrates the dynamic alterations in Δ[HbO], Δ[HHb], Δ[HbT], and the hemoglobin difference (Δ[HbD]= Δ[HbO]-Δ[HHb]) over a 5-minute forearm arterial occlusion. This graph expands on Figure 9 by introducing HbD, represented by the yellow line. The chart is segmented into baseline (0s-300s), arm cuff inflation (300s-600s), and cuff deflation (600s-780s),

demarcated by dashed red lines on the x-axis. Concentration values in µM, ranging from -10 to 8 µM, are depicted on the y-axis. Specifically gathered for 3cm data collection, refer to the appendix for 1cm data details. The anticipated trends reveal a gradual decrease in Δ[HbO], an increase in Δ[HHb], and relatively stable Δ[HbT] during the cuff phase, succeeded by swift returns to baseline levels in the 3-minute recovery. Notably, HbD exhibits a significant decrease during occlusion and compensatory elevation in the recovery phase.

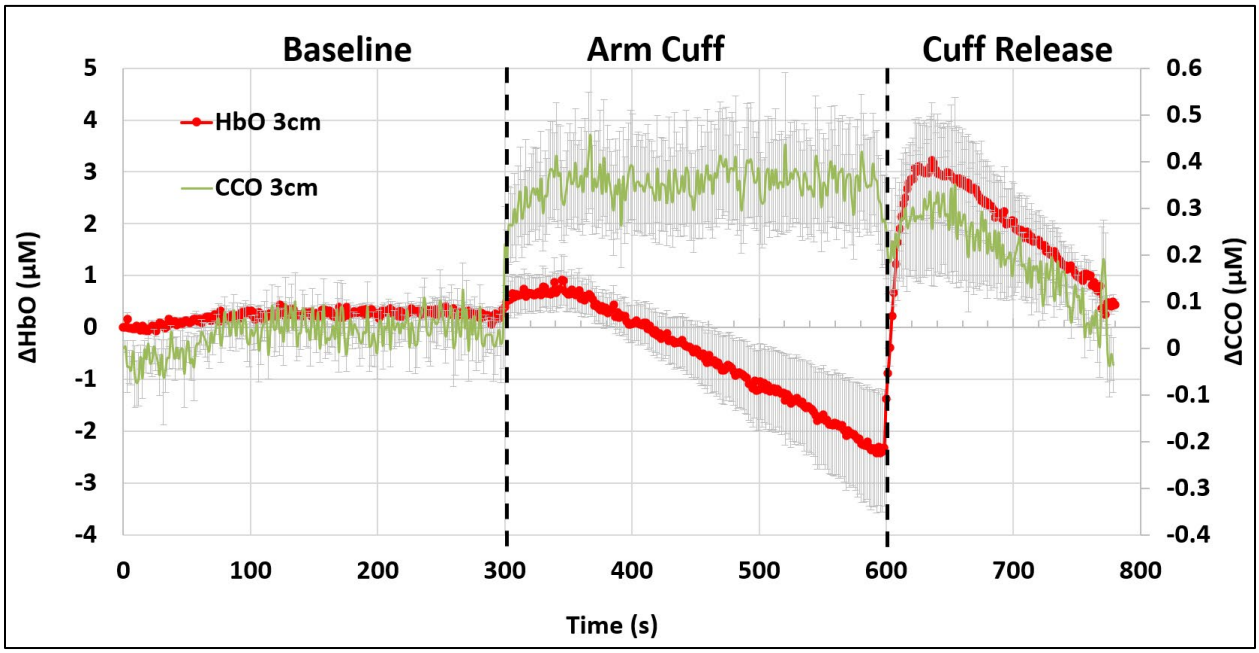

Figure 11. Dynamic changes in Δ HbO and ΔCCO Over Time.

In Figure 11, the alterations in Δ[CCO] are observed, showcasing a deviation from the trend exhibited by Δ[HbO] during the cuff period. The graph presents the concentrations of ΔHbO in µM (depicted in red) and ΔCCO in µM (depicted in green). Error bars, denoting upper and lower bounds for both ΔCCO and ΔHbO, are displayed in gray and represent the standard deviation of the global mean. The x-axis reflects time in seconds (0-780s), segmented into baseline, cuff

inflation, and cuff deflation, following the same protocol as in Figure 9. The left-hand y-axis indicates the concentration change in ΔHbO in μM, while the right-hand y-axis illustrates the concentration change in ΔCCO, ranging from 0.04 μM to 0.6 μM. Results indicate that ΔCCO rapidly adapted to the ischemic environment, decoupled from ΔHbO, maintained stability until occlusion release, and swiftly returned to baseline levels.

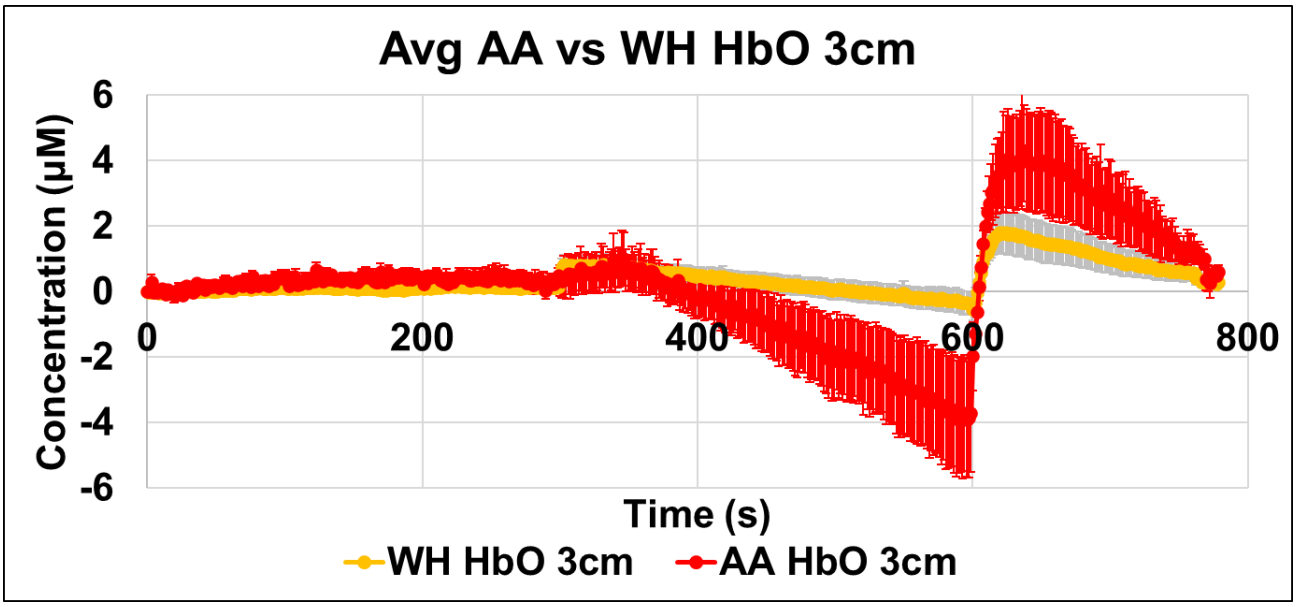

Figure 12. Average African American vs Caucasian ΔHbO Levels Over Time.

Figure 12 displays the average concentrations of ΔHbO in μM for AA and WH across time at a 3cm separation distance. The red line represents the concentration trend of AA ΔHbO μM over time at 3cm, accompanied by red upper and lower bound error bars. Similarly, the yellow line illustrates the concentration trend of WH ΔHbO μM over time at 3cm, with gray upper and lower bound error bars. Notably, a substantial decrease in oxygenated hemoglobin is observed in the AA population compared to the WH population during the arm occlusion period (300s-600s), followed by a heightened oxygen consumption in the recovery phase (600s-780s) compared to the WH

population. Concentration units are in µM, and error bars represent the standard deviation of the global mean for both AA and WH. The y-axis depicts the concentration change in ΔHbO from -6 to 6µM. The x-axis represents time in seconds (0-780s), following the same 3-segmentation protocol as in Figure 9.

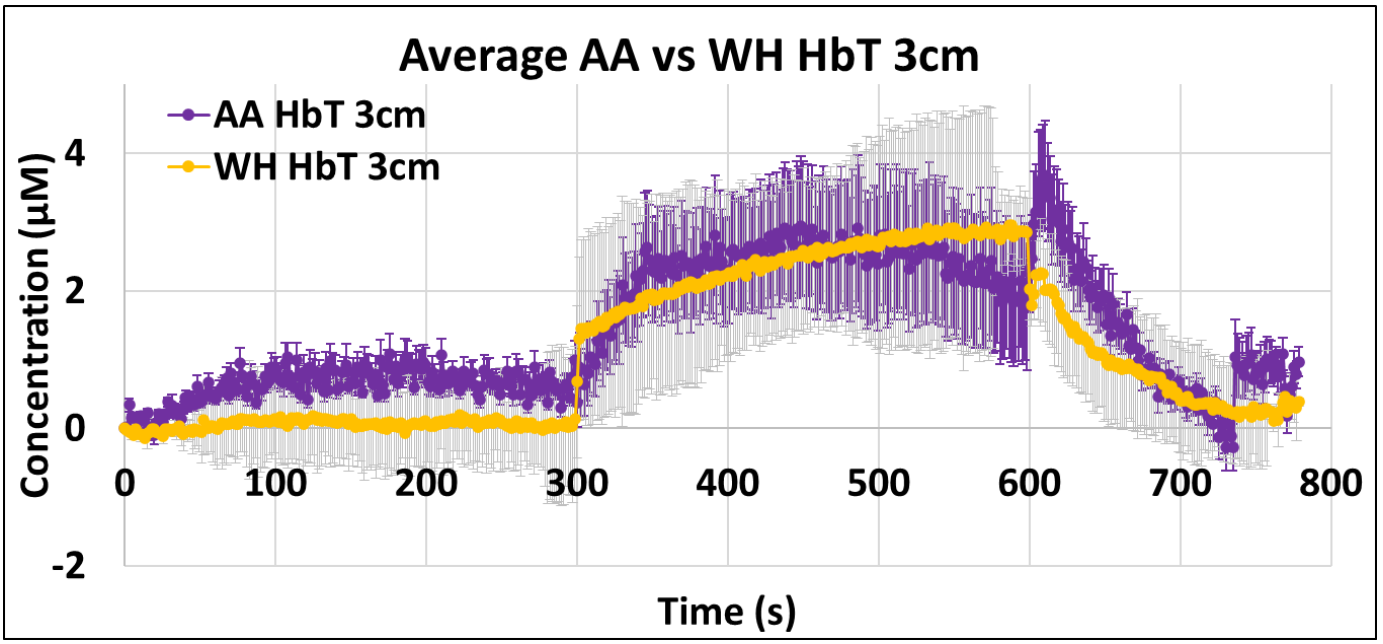

Figure 13. Average African American vs Caucasian Total Hemoglobin ΔHbT Over Time.

Figure 13 presents the average concentrations of total blood flow, calculated as HbT=[HbO]+[HHb], in µM for both AA and WH over time at a 3cm separation distance. The purple line depicts the concentration trend of AA ΔHbT µM over time at 3cm, accompanied by purple upper and lower bound error bars. Simultaneously, the yellow line illustrates the concentration trend of WH ΔHbT µM over time at 3cm, with gray upper and lower bound error bars. The error bars, representing upper and lower bounds for both AA and WH, reflect the standard deviation of each racial group. Notably, a sharp increase in blood flow is observed in the AA population compared to the WH population during the recovery period (600-780s), then gradual

returns to baseline. It is important to mention that there are overlapping error bars during both occlusion and recovery when both upper and lower bounds are considered. Concentration units are in μM, and error bars represent the standard deviation for both AA and WH. The y-axis depicts the concentration change in ΔHbT from -2 to 4μM, while the x-axis represents time in seconds (0-780s), following the same 3-segmentation protocol as in Figure 9.

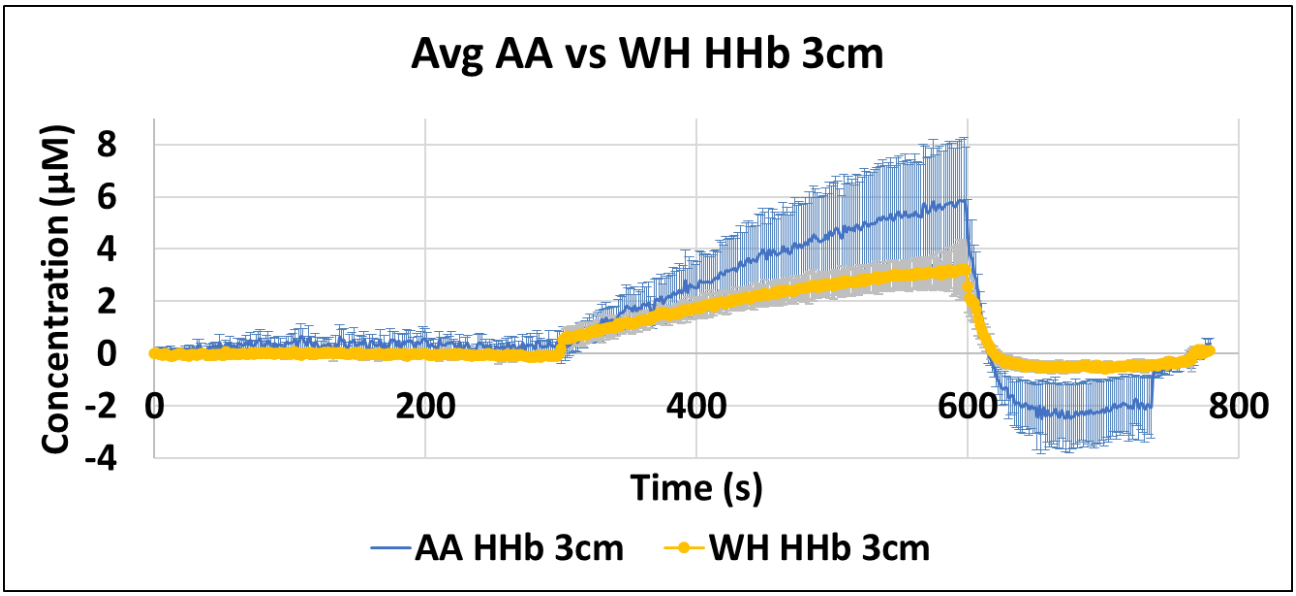

Figure 14. Average African American vs Caucasian ΔHHb Levels Over Time.

Figure 14 illustrates the average concentrations of ΔHHb in μM for both AA and WH over time at a 3cm separation distance. The blue line represents the concentration trend of AA ΔHHb μM over time at 3cm, accompanied by blue upper and lower bound error bars. Simultaneously, the yellow line illustrates the concentration trend of WH ΔHHb μM over time at 3cm, with gray upper and lower bound error bars. Notably, a significant increase in deoxygenated hemoglobin is observed in the AA population compared to the WH population during the arm occlusion period (300s-600s), followed by a sharp decline and a decreased concentration during the recovery phase (600s-780s) compared to the WH population, then returns to baseline. The y-axis depicts the concentration

change in ΔHHb from -4 to 8μM. The x-axis represents time in seconds (0-780s), following the same 3-segmentation protocol as in Figure 9.

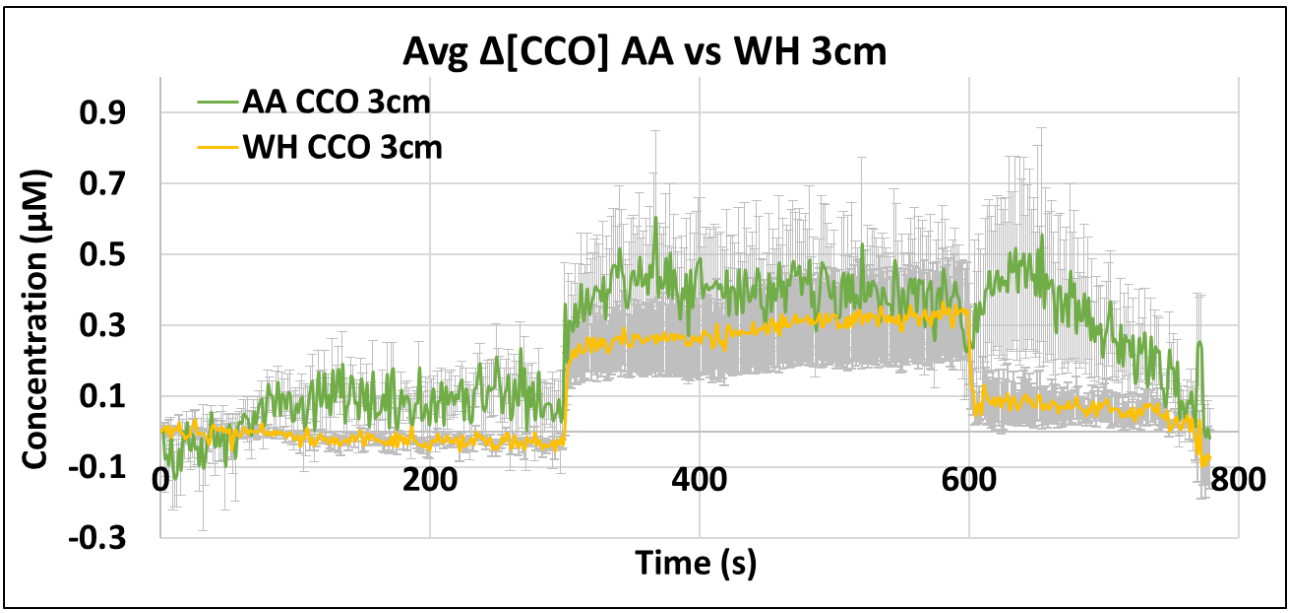

Figure 15. Average concentrations of African Americans versus Caucasians metabolic Cytochrome C Oxidases Δ[CCO] Levels Across Time.

Figure 15 illustrates the average concentrations of ΔCCO in μM for both AA and WH populations over time at a 3cm separation distance. The green line represents the concentration trend of AA ΔCCO μM over time, accompanied by green lower bound error bars. Simultaneously, the yellow line illustrates the concentration trend of WH ΔCCO μM over time, with gray upper bound error bars. The error bars, indicating upper and lower bounds for both AA and WH, reflect the standard deviation of each racial group. Importantly, there is significant difference in CCO concentration was observed during recovery where AA has a sharp increase and gradual return to baseline, however WH had a sharp decrease and plateau. Greater variance was observed in the AA population compared to the WH population during the arm occlusion period (300s-600s). The y-axis depicts the concentration change in ΔCCO from -0.3 to 0.9μM,

while the x-axis represents time in seconds (0-780s), following the same 3-segmentation protocol as in Figure 9.

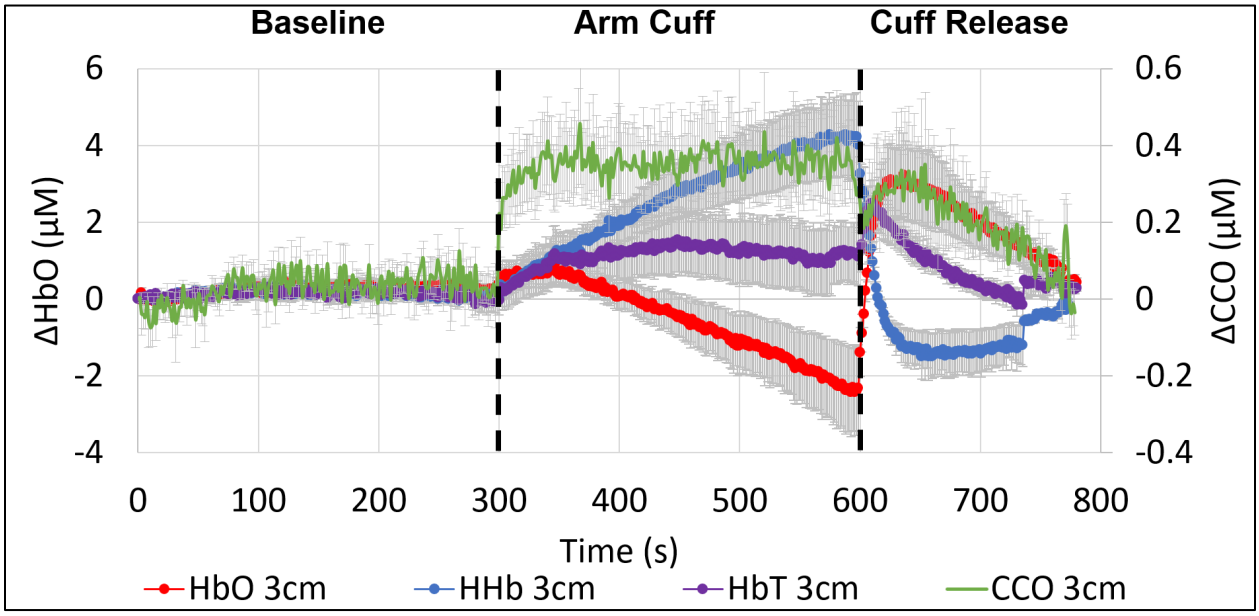

Figure 16. Average combined populations for HbO, HHb, HbT, and CCO Quantity Visualization Over Time.

Figure 16 shows the incorporated data of the global mean, offers a unified representation of HbO, HHb, CCO, and HbT over the course of the experimental protocol. This amalgamation provides a collective visualization of hemodynamic effects and averaged metabolic adaptations in response to the induced ischemic challenges. The left-hand y-axis is dedicated to the concentrations of HbO (depicted in red), HHb (depicted in blue), and HbT (depicted in purple), offering insight into the changes in oxygenation and overall hemoglobin levels. Simultaneously, the right-hand y-axis illustrates the concentrations of CCO (depicted in green), providing a specific focus on the metabolic component of the study. The x-axis, representing time in seconds, spans a total duration of 780 seconds, capturing the entire experimental timeline. All error bars,

depicted in gray, represent the global mean standard error of all 12 subjects at 3cm. This color-coded and error-bar-inclusive representation facilitates the examination of concurrent changes in both hemodynamic and metabolic parameters, enabling a holistic understanding of the physiological responses under investigation. The synchronized visualization of HbO, HHb, CCO, and HbT concentrations across time enhances the clarity of observed trends and aids in the interpretation of the intricate interplay between vascular dynamics and metabolic activity during the experimental protocol.

3.2 WTC Racial Results

The WTC graph shows phase shift and coupling of Hemodynamic and Metabolic for AA and WH over baseline, cuff occlusion, and recovery periods.

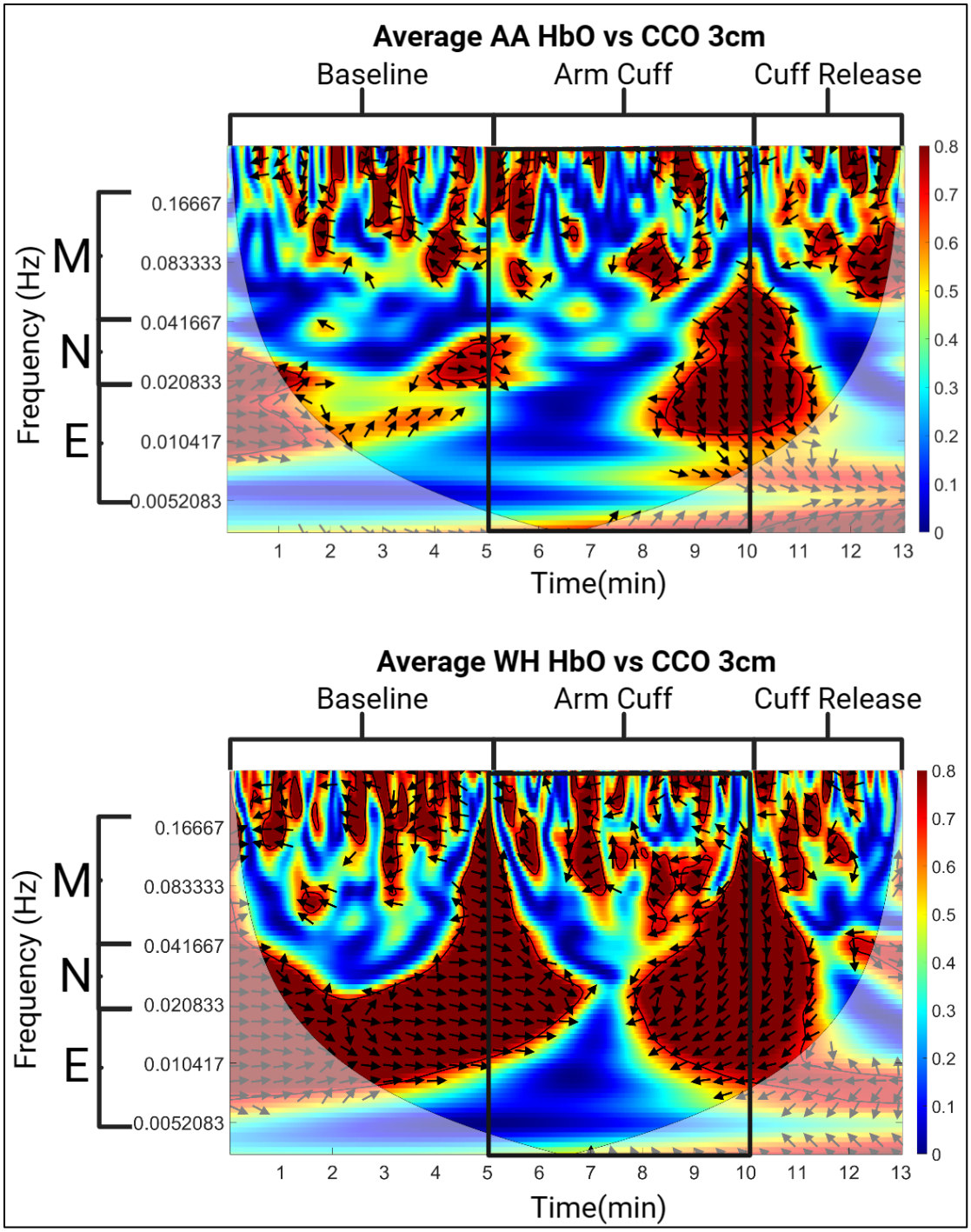

Figure 17. WTC Heat Maps for AA N=7 (top) and WH N=5 (bottom) Subjects Depicting Hemodynamic and Metabolic Correlation Over Baseline, Arm Cuff Occlusion, and Recovery, Across Three Infraslow Oscillation Frequencies Over Time.

In Figure 17, the Wavelet Transform Coherence (WTC) graphs are partitioned into three distinct sections: baseline (0 to 5 minutes), arm cuff application (5 to 10 minutes), and cuff release (10 to 13 minutes). The X-axis represents time in minutes, and the frequency range is denoted on the secondary Y-axis, with "M" for myogenic (0.16 to 0.04 Hz), "N" for neurogenic (0.04 to 0.02 Hz), and "E" for endogenic (0.02 to 0.005 Hz). This heat map illustrates the hemodynamic and metabolic coupling during the forearm occlusion protocol for both AA and WH groups. The occlusion time is highlighted with a black box to emphasize key activation and release time points of the arm cuff. The shadowed area at the edge of the heat maps represents the Cone of Interference (COI), accounting for the tapered nature of the Morlet wavelet, where padded zeros are added to each signal to ensure the inclusion of the first time-series point during Fourier Transform. Consequently, points within the COI, reflecting data at the edges of the continuous wavelet-transformed signals, are not considered in the WTC heat map analysis.

The color-coded heat map, ranging from 0 to 0.8 on the right Y-axis, reveals the coherence between hemodynamic and metabolic activity. Black arrows indicate phase shifts at 0° is in-phase, 180° signifying anti-phase, while 90° is positive coupling where HbO leads CCO, and 270° indicate decoupling where CCO leading HbO. Dark red areas signify high coherence activity, while blue areas suggest little to no coherence across the E/N/M bands. The WTC analysis was conducted for both AA and WH groups using averages, and no statistical analysis was performed due to limited knowledge of statistical processes for WTC.

Our WTC results unveiled three distinct features of coupling: in-phase coupling, decoupling, and anti-phase recoupling. During baseline and the initial occlusion phase, HbO and CCO were strongly in-phase coupled across three frequency bands (E/N/M) in WH, while weaker coupling was observed in AA. However, during occlusion, coupling between HbO and CCO decoupled

and shifted to anti-phase recoupling for WH, while AA exhibited a more extended period of complete decoupling. During recovery, both AA and WH groups gradually recoupled, AA becoming in-phase, and WH stayed anti-phase.

Chapter 4

4 Conclusion

4.1 Conclusion and Discussion of Hemodynamic-Metabolic Coupling

In conclusion, the findings of this study provide valuable insights into the physiological responses during FAO and its potential implications for cardiovascular health. The absence of observed mitochondrial dysfunction, as indicated by the comparable CCO fluctuations in both AA and WH populations, suggests a level of resilience in mitochondrial function during the induced ischemic challenges. This resilience may be attributed to the protective effects of FAO on mitochondrial dynamics and activity, reinforcing its potential as a therapeutic strategy for mitigating ischemic damage in various organs.

However, the study did uncover significant alterations in the E frequency bands, particularly in the AA population. The distinct decoupling patterns observed throughout baseline, occlusion, and recovery phases indicate a potential presence of ED in the healthy AA population. This highlights the sensitivity of the WTC method in detecting subtle changes in the coupling between hemodynamic and metabolic variables, specifically in the context of endothelial function.

The ability of bbNIRS to quantify dynamic alterations in Δ[HbO] and Δ[CCO] provided valuable information about the immediate adaptation of mitochondrial activity to the ischemic environment during FAO. The temporal coupling, decoupling, and recoupling observed between Δ[HbO] and Δ[CCO] during and after FAO, as revealed by WTC analysis, offer a nuanced understanding of the interplay between hemodynamic and metabolic responses in both populations.

While previous studies and algorithms have provided reassurance in understanding physiological responses, our investigation under FAO conditions, specifically hypoxia and ischemia, reveals inconsistencies in demand and supply dynamics. The interruptions in blood supply during these conditions trigger protective mechanisms within mitochondria [43,44,45]. Contrary to the expected inconsistencies, our study consistently reports observations that shed light on the nuanced and adaptive nature of mitochondrial responses during FAO. These findings challenge conventional expectations and contribute to a more comprehensive understanding of the intricate interplay between demand, supply, and the protective mechanisms enacted by mitochondria in the face of hypoxic and ischemic challenges.

The study also noted that, during baseline and the initial cuff stages, local vascular and metabolic activities were more closely in-phase coupled in WH compared to AA, indicating potential differences in the equilibrium between oxygen supply and demand. These results underscore the importance of considering racial and ethnic factors in studying the effects of FAO and its implications for cardiovascular health. In conclusion, this study provides valuable insights into the intricate interplay between hemodynamic and metabolic functions in diverse populations under ischemic stress [46,47]. Further research is crucial to unravel the specific mechanisms underlying these racial distinctions, fostering a comprehensive understanding of vascular responses and oxygen utilization in varying populations.

While these findings shed light on the mechanism of FAO, it is crucial to recognize the preliminary nature of this study. Further research is underway to validate and expand upon these observations, particularly in oxygen-deficient environments. The promising nature of the WTC method in monitoring preconditioning effects on ED opens new avenues for investigating protective mechanisms against CVD.

4.2 Discussion

4.3 Hemodynamic Trends

Figure 9 presents a comprehensive view of dynamic alterations in oxygenated hemoglobin ΔHbO, ΔHHb, and total hemoglobin concentration ΔHbT. The observed results in this study align with previously established trends, reflecting the inverse relationship between ΔHbO and ΔHHb during arterial occlusion. The red line illustrates a gradual decrease in ΔHbO, indicating reduced oxygenated hemoglobin levels, while the blue line demonstrates an increase in ΔHHb, representing elevated deoxygenated hemoglobin levels. Importantly, the purple line depicting ΔHbT remains relatively constant during the cuff application, emphasizing the stability of total hemoglobin concentration throughout this ischemic challenge.

These findings are consistent with established literature and algorithms, further validating the reliability of the methodology employed in this study. The observed trends during occlusion are indicative of the expected physiological responses to reduced blood flow and oxygen supply, with a concurrent increase in deoxygenated hemoglobin. Following the initial cuff release, a rapid return of the parameters to baseline levels is noted during the 3-minute recovery period. This swift recovery underscores the dynamic adaptability of the vascular system to changes in blood flow,

with a prompt restoration of oxygenated hemoglobin levels and a concurrent decrease in deoxygenated hemoglobin.

Figure 9 contributes to the existing body of knowledge by reaffirming the inverse relationship between ΔHbO and ΔHHb during arterial occlusion, as well as the stability of ΔHbT. The observed trends align with established physiological responses to ischemic challenges, emphasizing the robustness of the vascular system in maintaining hemodynamic equilibrium.

4.4 Oxygenated Hemoglobin and Cytochrome C Oxidase Independency

The findings presented in Figure 11 reveal intriguing insights into the dynamics of ΔCCO concentrations in response to induced ischemic challenges, particularly when juxtaposed with the alterations in ΔHbO. Notably, the concentrations of ΔCCO, depicted in green, exhibit a distinct pattern that deviates from the established trends observed in ΔHbO during the cuff period.

One notable aspect is the scale of concentrations, where ΔCCO concentrations are approximately one-tenth of ΔHbO concentrations. This marked difference underscores the ability of our sophisticated bbNIRS chromophore algorithm to effectively separate and quantify these chromophores, providing a nuanced understanding of the metabolic and hemodynamic responses in hypoxic environments.

The observed deviation in ΔCCO concentrations during the cuff period is particularly noteworthy. While ΔHbO experiences a steep decline due to the occlusion, reflecting the decrease in oxygenated blood flow, ΔCCO maintains stability until the release of the cuff. This stability in ΔCCO suggests a potential protective mechanism aimed at preserving metabolic function even when hemodynamic functions, represented by ΔHbO, are significantly impacted.

During the occlusion phase, a unique metabolic response is observed. ΔCCO exhibits a sharp increase from baseline (0-0.2 μM) but then plateaus steadily, indicating a controlled and adaptive metabolic adjustment to the ischemic environment. In contrast, once the cuff is released, ΔCCO increases to 0.5 μM and steadily returns to baseline levels, suggesting an overshoot and gradual return to the baseline metabolic state. This pattern of ΔCCO responses challenges the conventional expectations in the field, as it diverges from the trends typically associated with hypoxic conditions. The uncoupling of ΔCCO from the steep decline in ΔHbO during the occlusion phase suggests that metabolic protective measures may be distinct from hemodynamic functions in response to induced ischemia.

The rapid adaptation and stability of ΔCCO concentrations under hypoxic conditions offer a novel perspective on the potential protective mechanisms orchestrated by metabolism to ensure the continuity of metabolic processes. While ΔHbO responds to the heightened demand for blood flow, ΔCCO exhibits a controlled response, avoiding overcompensation during hypoxic challenges.

These results emphasize the significance of our bbNIRS chromophore algorithm in unraveling the intricate interplay between metabolic and hemodynamic functions. The ability to separate these concentrations opens new avenues for studying the specific contributions of metabolism and hemodynamics during ischemic conditions. FAO emerges as a valuable mechanism for investigating the protective measures of metabolism independent of hemodynamic fluctuations. The unique responses of ΔCCO observed in this study pave the way for a deeper understanding of how metabolism adapts to and protects against hypoxic challenges, offering potential implications for therapeutic interventions in ischemic scenarios.

In addition to the insights provided by our novel findings on ΔCCO concentrations, it is crucial to emphasize the unique aspect of our bbNIRS chromophore algorithm in discerning the intricate

relationship between ΔHbO and ΔCCO. Our results stand out from previous research, which often reported consistent and proportionate relationships between HbO and CCO concentrations under hypoxic conditions. In contrast, our study unveils an inversely proportional relationship, underscoring the heightened sensitivity of our algorithm to chromophore changes.

This distinct ability to discriminate between chromophores presents a valuable tool for dissecting the complex dynamics of oxygenation and mitochondrial activity. The inverse relationship between HbO and CCO concentrations observed in our study may signify a previously unrecognized protective mechanism within mitochondrial physiology. The rapid and adaptive response of metabolic activity, as observed in both AA and WH individuals, suggests a concerted effort to safeguard and sustain limb metabolic function under challenging hypoxic conditions.

The adaptive resilience highlighted by distinct chromophore changes unveils an intricate mechanism orchestrated by mitochondria to ensure the continued availability of metabolic resources in response to fluctuating oxygen levels. This observation opens new avenues for understanding mitochondrial adaptations and their implications for metabolic stability in ischemic scenarios. The ability of our algorithm to capture these nuanced relationships between chromophores enhances our understanding of the interplay between metabolic and hemodynamic functions, providing valuable insights into the protective measures employed by mitochondria in response to hypoxic challenges.

4.5 Characteristics of Oxygenated Hemoglobin Dynamic Changes Over Time.

The dynamic changes in ΔHbO concentrations, as depicted in Figure 12, reveal intriguing racial disparities during arterial occlusion and recovery for AA and WH populations. While no significant differences were observed in ΔHbO concentrations during the baseline period, the induced

ischemic challenge brought forth notable variations, shedding light on the unique hemodynamic responses of each racial group.

During the arm occlusion period (300s-600s), AA individuals exhibited a substantial and rapid decline in ΔHbO, reaching a significant difference of -4.0μM from baseline. In contrast, WH individuals displayed a more gradual decline, with a difference ranging from 1 to -0.5μM. This significant difference in ΔHbO during occlusion suggests a potential disparity in hemodynamic demand and oxygen utilization between AA and WH populations.

The steeper and faster decline in ΔHbO observed in AA individuals may indicate a heightened oxygen demand during the occlusion phase, possibly reflecting increased metabolic activity or vasomotor responses specific to this racial group. The more gradual decline in ΔHbO in WH individuals suggests a different pattern of oxygen utilization, possibly indicative of a more efficient vascular response in this population.

Upon cuff release and during the recovery phase (600s-780s), AA individuals demonstrated an overshoot in ΔHbO, surpassing the levels needed to return to baseline. This overshoot was followed by a steeper slope in the return to baseline. In contrast, WH individuals exhibited a more controlled and steady increase in ΔHbO during recovery, with a gradual and consistent return to baseline.

These observed differences underscore the complexity of hemodynamic responses to ischemic challenges in diverse racial populations. The significant decline in ΔHbO in AA individuals during occlusion and the subsequent overshoot during recovery suggest potential variations in metabolic and vascular regulation. Further investigations into the underlying physiological mechanisms

driving these differences are warranted to deepen our understanding of racial distinctions in oxygen utilization and vascular dynamics under ischemic conditions.

Several factors may contribute to these observed racial disparities in ΔHbO, including potential variations in vascular reactivity, oxygen utilization, metabolic activity, mitochondrial function, and microcirculation. Additionally, environmental and lifestyle factors should be considered, as they can significantly impact vascular health and oxygen metabolism. Further research is essential to unravel the intricate interplay of these factors and determine their specific contributions to the observed racial disparities in ΔHbO, providing valuable insights into the complex relationship between vascular dynamics, oxygen utilization, and metabolic responses in diverse populations under ischemic stress.

4.6 Characteristics of Deoxygenated Hemoglobin Dynamic Changes Over Time.

The outcomes illustrated in Figure 14 reveal compelling distinctions between AA and WH populations during induced ischemic challenges, shedding light on the intricate interplay of vascular and metabolic responses. Notably, substantial differences were observed in deoxygenated hemoglobin levels (ΔHHb) between AA and WH individuals, particularly during the arm occlusion period (300s-600s). The notable increase in ΔHHb for AA individuals during occlusion suggests a distinctive hemodynamic response, possibly indicating a more pronounced vasoconstrictive effect or altered oxygen utilization within the AA group.

In the subsequent recovery phase (600s-780s), AA individuals exhibited a sharp decline and decreased concentration of ΔHHb compared to WH individuals. This distinctive recovery trajectory in AA individuals implies a nuanced response, potentially reflecting delayed vascular

adjustments or a unique metabolic recovery process. In contrast, WH individuals displayed a gradual incline in ΔHHb during occlusion, followed by a consistent and rapid return to baseline, suggesting a more efficient vascular response and a prompt restoration of normal metabolic function.

These findings underscore the complexity of hemodynamic responses in diverse racial groups during and after induced ischemic conditions. The observed variations in ΔHHb concentrations emphasize the necessity for a deeper understanding of the underlying physiological mechanisms governing vascular dynamics and oxygen utilization. Several factors may contribute to these racial distinctions, including variations in vascular reactivity, oxygen utilization within muscle tissue, microcirculation differences, and unique adaptive responses to ischemic conditions.

Considering the potential influence of evolutionary adaptations, environmental factors, and hemoglobin variations, it becomes essential to explore the multifaceted aspects contributing to these disparities. Additionally, environmental and genetic factors, such as diet, physical activity levels, and environmental exposures, warrant consideration for their potential impact on vascular health and oxygen metabolism, contributing to the observed differences in ΔHHb between AA and WH populations.

4.7 Characteristics of Total Hemoglobin Blood Flow Dynamic Changes Over Time.

The results depicted in Figure 13 provide insight into the temporal dynamics of total blood flow (HbT) concentrations in response to induced ischemic challenges for both AA and WH populations. Despite the absence of a statistically significant difference, subtle trends emerge, suggesting potential variations in the hemodynamic responses between the two groups.

During the arm occlusion period (300s-600s), a noteworthy observation is the slight decrease in blood flow observed in the AA population compared to their WH counterparts. While this difference does not reach statistical significance, it hints at potential variations in vascular responses during ischemia. This slight reduction in blood flow in AA individuals may be attributed to differences in vascular reactivity, endothelial function, or oxygen utilization within muscle tissues.

Upon cuff release, AA experienced a sharp increase in blood flow during the recovery phase (600s-780s). Interestingly, the response in the WH population decreased gradually until baseline, suggesting a faster adjustment to the increased hemodynamic demand. This discrepancy in the recovery trajectory might imply distinct vascular dynamics and adaptive responses between the two racial groups.

The observed overlapping error bars during both occlusion and recovery periods highlight the variability within each population and the need for caution when interpreting these trends. While the concentration trends and subtle differences suggest potential variations in blood flow dynamics between AA and WH individuals, the lack of statistical significance underscores the complexity of hemodynamic responses in diverse populations.

It is crucial to consider that these findings represent a snapshot of the interplay between hemodynamic and metabolic functions during induced ischemia. The nuanced variations observed in total blood flow concentrations hint at potential racial distinctions in vascular responses, urging further investigation into the underlying physiological mechanisms that contribute to these trends.

4.8 Characteristics of Hemoglobin Differences Dynamic Changes Over Time.

The introduction of HbD (hemoglobin difference) in Figure 10 offers a comprehensive perspective on the dynamic alterations in hemoglobin concentrations during a 5-minute forearm arterial occlusion. HbD, represented by the yellow line, plays a crucial role in assessing the total change in blood flow concentration, allowing for a nuanced understanding of differences during occlusion and compensatory responses in the recovery phase. During the cuff phase, a gradual decrease in ΔHbO reflects the reduction in oxygenated hemoglobin, while an increase in ΔHHb indicates a rise in deoxygenated hemoglobin. Notably, ΔHbT remains relatively stable, emphasizing the intricate balance between these hemoglobin components.

HbD exhibits a significant decrease during occlusion, capturing the combined effect of reduced oxygenated hemoglobin and increased deoxygenated hemoglobin. This decline in HbD signifies a comprehensive response to the ischemic challenge, highlighting the impact on blood flow and oxygenation in the measured region. As the cuff is deflated and the recovery phase unfolds, compensatory mechanisms come into play. ΔHbO swiftly returns to baseline levels, indicating a prompt response to the restoration of blood flow. In contrast, ΔHHb undergoes a compensatory elevation, possibly reflecting an overshoot in deoxygenated hemoglobin. Crucially, HbD demonstrates a compensatory elevation in the recovery phase, emphasizing its role in capturing the overall hemodynamic response.

The observed dynamics in HbD, with a significant decrease during occlusion followed by a compensatory elevation in recovery, provide valuable insights into the complex interplay of oxygenated and deoxygenated hemoglobin during ischemic challenges. This nuanced understanding contributes to the broader comprehension of hemodynamic responses and highlights

the significance of considering the total hemoglobin difference in studying vascular dynamics under challenging conditions.

4.9 Characters of Cytochrome C Oxidases Dynamic Changes Over Time.

The results depicted in Figure 15 shed light on the temporal dynamics of CCO concentrations in response to arterial occlusion and recovery for both AA and WH populations. Notably, our analysis revealed no significant statistical differences between AA and WH during occlusion, as the standard error bars for ΔCCO concentrations exhibited overlapping trends. During baseline, slight differences can be observed between AA and WH, which becomes more pronounced during recovery. While the absence of pronounced divergence in occlusion suggests a shared resilience in mitochondrial function. An intriguing observation emerged with greater variance evident in the AA population during the arm occlusion period (300s-600s) compared to their WH counterparts.

The nuanced recovery dynamics in the AA population, characterized by a prolonged return to baseline, hint at potential factors influencing mitochondrial adaptability. This prolonged recovery in AA individuals was further accompanied by an overcompensation in hemodynamic blood flow, indicating a distinctive response pattern compared to WH individuals. Our study provides valuable insights into the temporal dynamics of CCO concentrations during induced ischemic challenges, highlighting both similarities and subtle distinctions between AA and WH populations.

The rapid adaptation and stable behavior of CCO concentrations observed under hypoxic conditions offer intriguing insights into a potential mitochondrial protective mechanism designed to preserve metabolic function. This consistent and swift response of CCO, despite induced ischemic challenges, suggests an adaptive resilience in mitochondrial activity crucial for maintaining cellular homeostasis. The observed inverse relationship between HbO and CCO

concentrations, facilitated by our sophisticated bbNIRS chromophore algorithm, introduces a novel perspective on the interplay between hemodynamic and metabolic functions.

4.10 Characteristics of the Wavelet Transform Coherence Between Hemodynamic and Metabolic Coupling in African American and Caucasians.

The WTC algorithm for AA involved in putting the HbO signal first, where a leading phase of HbO creates a 45° angle, while a following phase results in a negative angle, suggesting potential precedence of CCO vibrations followed by HbO. Equilibrium, indicated by 0° or 180° phase shifts, was observed in the baseline data for both AA and WH populations. Notably, in the AA population, WTC revealed significant decoupling in the Endogenic frequency bands, particularly in the during occlusion, suggesting prevalent endothelial dysfunction exacerbated by ischemic events. This decoupling, initiated during baseline, intensified during occlusion, and the re-establishment of coupling was delayed, gradually returning to an in-phase configuration in the recovery phase. This intricate pattern extended into the neurogenic band, highlighting dynamic vascular responses. While the M band shows intermitted coupling and decoupling in anti-phase through the time series.

In the WH population, robust coupling between hemodynamic and metabolic variables was observed across all frequency bands, particularly in the endothelial frequency. A persistent in-phase coupling remained consistent until the midpoint of occlusion, where a noticeable transition toward an out-of-phase and decoupled state occurred. Interestingly, this decoupling was transient, responding promptly to the occlusion stimulus, and the coupling rapidly re-established, returning to an in-phase configuration during the recovery phase. This intricate pattern extended into the neurogenic band, emphasizing dynamic vascular responses.

The unique observation of in-phase coupling, decoupling, and anti-phase recoupling features during cuff occlusion provides insight into the underlying physiology of metabolic-vascular coupling in oxygen-deficient environments. These features may serve as markers for vascular health, shedding light on the dynamic interactions between mitochondrial and vascular oscillations in response to ischemic challenges.

4.11 Limitations

This study encountered limitations related to participant numbers, despite maintaining an equivalent representation of African American and Caucasian individuals. To bolster the robustness of the findings, a larger and more diverse cohort is warranted. The classification of race relied on participants self-reporting their parental race, introducing a potential source of inaccuracy in capturing the genetic diversity within fully African American or Caucasian subjects. While acknowledging this limitation, addressing the intricacies of genetic diversity was beyond the scope of the current study.

A potential limitation lies in our algorithm, which incorporates μa and μs values for the forearm, and there may be biases based on race or gender. However, for the sake of consistency, our study utilized the same μa and μs values for both racial and gender comparisons. Further literature analysis is needed to determine if μa and μs values differ by melanin content, which falls beyond the scope of this study.

Recognizing gender distribution as a crucial factor in CVD prevalence, this study demonstrated a gender imbalance, with a disproportionate representation of 9 females and 3 males across both populations. The skewed gender distribution may impact the generalizability of the findings, and

future research endeavors should strive for a more balanced representation to explore potential gender-specific variations in responses to interventions. Although gender comparisons were conducted, they were subsequently excluded.

The quantification of the occlusion event posed a challenge due to the dynamic nature of the series, limiting comprehensive statistical analyses. To address this limitation, the study employed WTC analysis to capture intricate dynamics. It is essential to acknowledge that, while WTC analysis provides valuable insights, further dedicated statistical analyses are required to unveil nuanced and statistically meaningful differences associated with the occlusion event. Future research efforts should encompass a broader array of statistical tools for a comprehensive understanding of the observed phenomena.

4.12 Future work

Building on the insights gained from this study, future research endeavors will extend the investigation to the temporal artery, exploring hemodynamic-metabolic coupling within the prefrontal cortex with a specific focus on stroke prevention. This expansion aims to broaden the understanding of the physiological responses associated with FAO in a different vascular context, with potential implications for stroke prevention strategies.

It's crucial to recognize the complexity of these responses and the multifaceted nature of vascular and metabolic interactions. Further research, encompassing molecular and physiological investigations, is essential to unravel the specific mechanisms underlying these disparities. This study offers a steppingstone for deeper exploration into the intricate dynamics of vascular and

metabolic responses during ischemia in diverse populations, paving the way for a more comprehensive understanding of the observed variations in deoxygenated blood levels.

The upcoming study will encompass measurements of hemodynamic and metabolic parameters, employing the established techniques of bbNIRS and WTC analysis. Notably, this future work is designed to rectify the gender disparity observed in the current study, ensuring a balanced representation of both male and female participants to enhance the generalizability of findings. The ongoing nature of this research positions it as an evolving exploration into the applications of FAO, bbNIRS, and WTC analysis. As new insights emerge, this research will contribute to the collective understanding of vascular responses and guide the development of targeted interventions for stroke prevention. The dedication to equal gender representation reflects a commitment to comprehensively exploring potential gender-specific nuances in the outcomes of interventions.

References

1. F. Coronado, S. C. Melvin, R. A. Bell, and G. Zhao, "Global Responses to Prevent, Manage, and Control Cardiovascular Diseases," Prev. Chronic Dis., vol. 19, p. 220347, 2022. [Online]. Available: http://dx.doi.org/10.5888/pcd19.220347
2. J. He et al., "Trends in Cardiovascular Risk Factors in US Adults by Race and Ethnicity and Socioeconomic Status, 1999-2018," JAMA, vol. 326, no. 13, pp. 1286–1298, 2021, doi: 10.1001/jama.2021.15187.
3. Q. R. Youmans et al., "Disparities in Cardiovascular care: Past, present, and solutions," Cleveland Clinic Journal of Medicine, vol. 86, no. 9, pp. 621–632, Sep. 2019, doi: 10.3949/ccjm.86a.18088.
4. H.-J. Sun, Z.-Y. Wu, X.-W. Nie, and J.-S. Bian, "Role of endothelial dysfunction in cardiovascular diseases: The link between inflammation and hydrogen sulfide," Frontiers, https://www.frontiersin.org/articles/10.3389/fphar.2019.01568/full (accessed Nov. 30, 2023).
5. D. Tousoulis, C. Antoniades, and C. Stefanadis, "Evaluating endothelial function in humans: a guide to invasive and non-invasive techniques," Heart, vol. 91, no. 4, 2005. [Online]. Available: https://heart.bmj.com/content/91/4/553.
6. G. Morris, B. K. Puri, L. Olive, A. Carvalho, M. Berk, K. Walder, L. T. Gustad, and M. Maes, "Endothelial dysfunction in neuroprogressive disorders—causes and suggested treatments," BMC Medicine, vol. 18, Article number: 305, 2020. [Online]. Available: https://bmcmedicine.biomedcentral.com/articles/10.1186/s12916-020-01749-w.

7. Y.-P. Li, Z.-X. Fan, J. Gao, X.-P. Sun, G.-H. Zhu, Y.-H. Zhang, J. Si, X.-B. Zuo, Z. Liu, Q. Hua, and J. Li, "Influencing factors of vascular endothelial function in patients with non-obstructive coronary atherosclerosis: a 1-year observational study," BMC Cardiovascular Disorders, vol. 20, Article number: 40, 2020. [Online]. Available: https://bmccardiovascdisord.biomedcentral.com/articles/10.1186/s12872-020-01326-2.
8. V. J. Mancilla, N. C. Peeri, T. Silzer, R. Basha, M. Felini, H. P. Jones, N. Phillips, M.-H. Tao, S. Thyagarajan, and J. K. Vishwanatha, "Understanding the Interplay Between Health Disparities and Epigenomics," Front. Genet., vol. 11, 2020. [Online]. Available: https://www.frontiersin.org/articles/10.3389/fgene.2020.00903/full.
9. Health Disparities: African Americans/Blacks," Centers for Disease Control and Prevention, 2023. [Online]. Available: https://www.cdc.gov/nchhstp/healthdisparities/africanamericans.html.
10. L. Jack Jr, "Advancing Health Equity, Eliminating Health Disparities, and Improving Population Health," Prev Chronic Dis, vol. 18, 2021. [Online]. Available: https://www.cdc.gov/pcd/issues/2021/21_0264.htm.
11. Gokce, N., Holbrook, M., Duffy, S. J., Demissie, S., Cupples, L. A., Biegelsen, E., Keaney Jr, J. F., Loscalzo, J., & Vita, J. A. (2001). Effects of Race and Hypertension on Flow-Mediated and Nitroglycerin-Mediated Dilation of the Brachial Artery.
12. Martin ZT, Al-Daas IO, Cardenas N, Kolade JO, Merlau ER, Vu JK, Brown KK, Brothers RM. Peripheral and Cerebral Vascular Reactivity in Black and White Women: Examining the Impact of Psychosocial Stress Exposure Versus Internalization and Coping. medRxiv [Preprint]. 2023 Mar 17:2023.03.16.23287388.doi: 10.1101/2023.03.16.23287388. PMID: 36993407; PMCID: PMC10055599.

13. Y. Hao, M. Xin, L. Feng, X. Wang, X. Wang, D. Ma, and J. Feng, “Review Cerebral Ischemic Tolerance and Preconditioning: Methods, Mechanisms, Clinical Applications, and Challenges,” Front. Neurol., vol. 11, 2020. [Online]. Available: https://www.frontiersin.org/articles/10.3389/fneur.2020.00812/full.
14. S. Y. Lim and D. J. Hausenloy, “Forearm Arterial Occlusion: from bench to bedside,” Front. Physiol., vol. 3, 2012. [Online]. Available: [https://doi.org/10.3389/fphys.2012.00027].
15. M. Donato, E. P. Bin, V. D’Annunzio, and R. J. Gelpi, “Myocardial remote ischemic preconditioning: from cell biology to clinical application,” Mol. Cell. Biochem., 2021. [Online]. Available: https://doi.org/10.1007/s11010-021-04192-4.
16. X. Ji, W. Zhao, J. Boltze, S. Li, R. Meng, Y. Wang, G. J. Bix, C. V. Borlongan, J. M. Gidday, S. Koch, J. C. Quindry, R. R. Ratan, K. Veighey, G. Xi, G. Pignataro, D. C. Hess, and D. J. Hausenloy, “Clinical practice guidelines of Forearm Arterial Occlusion for the management of cerebrovascular diseases,” Conditioning Medicine, vol. 2, no. 5, pp. 225-241, 2019. [Online]. Available: https://doi.org/10.18332/tid/162366.
17. D. J. Hausenloy and D. M. Yellon, “Remote ischaemic preconditioning: underlying mechanisms and clinical application,” Cardiovascular Research, vol. 79, no. 3, pp. 377-386, Aug. 2008. [Online]. Available: https://doi.org/10.1093/cvr/cvn114. Sure, here is the IEEE citation for the article you provided:
18. C. Dezfulian, M. Garrett, and N. R. Gonzalez, “Clinical application of preconditioning and postconditioning to achieve neuroprotection,” Transl Stroke Res, vol. 4, no. 1, pp. 19-24, Feb. 2013. [Online]. Available: https://doi.org/10.1007/s12975-012-0224-3. PMID: 24323188; PMCID: PMC4224593.

19. Y. Li, J. Sun, R. Wu, J. Bai, Y. Hou, Y. Zeng, Y. Zhang, X. Wang, Z. Wang, and X. Meng, “Mitochondrial MPTP: A Novel Target of Ethnomedicine for Stroke Treatment by Apoptosis Inhibition,” Front Pharmacol, vol. 11, 2020. [Online]. Available: https://doi.org/10.3389/fphar.2020.00352. PMID: 32269527; PMCID: PMC7109312.
20. D. J. Hausenloy, M. Ntsekhe, and D. M. Yellon, "A future for remote ischaemic conditioning in high-risk patients," Basic Res Cardiol, vol. 115, p. 35, 2020. [Online]. Available: https://doi.org/10.1007/s00395-020-0794-2
21. Limb Forearm Arterial Occlusion: Mechanisms, Anesthetics, and the Potential for Expanding Therapeutic Options," Front. Neurol., vol. 9, sec. Stroke, Feb. 2018. [Online]. Available: https://doi.org/10.3389/fneur.2018.00040
22. M. Donato, E. P. Bin, V. D´Annunzio, et al., "Myocardial remote ischemic preconditioning: from cell biology to clinical application," Mol Cell Biochem, vol. 476, pp. 3857-3867, 2021. [Online]. Available: https://doi.org/10.1007/s11010-021-04192-4
23. C. Rocca, T. Soda, E. M. De Francesco, et al., "Mitochondrial dysfunction at the crossroad of cardiovascular diseases and cancer," J Transl Med, vol. 21, p. 635, 2023. [Online]. Available: https://doi.org/10.1186/s12967-023-04498-5
24. J. Sadoshima, R. N. Kitsis, and S. Sciarretta, "Editorial: Mitochondrial Dysfunction and Cardiovascular Diseases," Front. Cardiovasc. Med., vol. 8, sec. Cardiovascular Metabolism, Jan. 2021. [Online]. Available: https://doi.org/10.3389/fcvm.2021.645986
25. C. Robba, D. Battaglini, C. S. Samary, et al., "Ischaemic stroke-induced distal organ damage: pathophysiology and new therapeutic strategies," ICMx, vol. 8, suppl. 1, p. 23, 2020. [Online]. Available: https://doi.org/10.1186/s40635-020-00305-3

26. Liang J, Han R, Zhou B. Metabolic Reprogramming: Strategy for Ischemic Stroke Treatment by Ischemic Preconditioning. Biology (Basel). 2021 May 11;10(5):424. doi: 10.3390/biology10050424. PMID: 34064579; PMCID: PMC8151271.

27. Pruitt, T.; Carter, C.; Wang, X.; Wu, A.; Liu, H. Photobiomodulation at Different Wavelengths Boosts Mitochondrial Redox Metabolism and Hemoglobin Oxygenation: *Lasers* vs. *Light-Emitting Diodes In Vivo*. *Metabolites* 2022, *12*, 103. https://doi.org/10.3390/metabo12020103

28. H. Renguul, "Physiological Analyses of Broadband Near-Infrared Spectroscopy and Electrophysiological Measurements in Vivo for Biomedical Applications." Order No. 30593078, The University of Texas at Arlington, United States -- Texas, 2023.

29. S. Shahdadian, X. Wang, S. Kang, C. Carter, A. Chaudhari, and H. Liu, "Prefrontal cortical connectivity and coupling of infraslow oscillation in the resting human brain: a 2-channel broadband NIRS study," Cereb Cortex Commun, vol. 3, no. 3, 2022. [Online]. Available: [https://doi.org/10.1093/texcom/tgac033]. PMID: 36072711; PMCID: PMC9441674.

30. C. Sissons, F. Saeed, C. Carter, K. Lee, K. Kerr, S. Shahdadian, and H. Liu, "Unilateral Mitochondrial–Hemodynamic Coupling and Bilateral Connectivity in the Prefrontal Cortices of Young and Older Healthy Adults," Bioengineering, vol. 10, 2023. [Online]. Available: https://doi.org/10.3390/bioengineering10111336.

31. S. Shahdadian, X. Wang, S. Kang, C. Carter, and H. Liu, "Site-specific effects of 800- and 850-nm forehead transcranial photobiomodulation on prefrontal bilateral connectivity and unilateral coupling in young adults," Neurophotonics, vol. 10, no. 2, 2023. [Online].

Available: https://doi.org/10.1117/1.NPh.10.2.025012. PMID: 37284247; PMCID: PMC10240350.

32. Z. Ben Taleb, D. Dabroy, J. Akins, M. D. Nelson, M. E. Kalan, and M. Rezk-Hann, “Pod-based e-cigarettes versus combustible cigarettes: The impact on peripheral and cerebral vascular function and subjective experiences,” Tob. Induc. Dis., vol. 21, May 2023. [Online]. Available: https://doi.org/10.18332/tid/162366.

33. P. Phan, D. Highton, S. Brigadoi, I. Tachtsidis, M. Smith, and C. E. Elwell, "Spatial Distribution of Changes in Oxidised Cytochrome C Oxidase During Visual Stimulation Using Broadband Near Infrared Spectroscopy Imaging," in Oxygen Transport to Tissue XXXVIII, Q. Luo, L. Li, D. Harrison, H. Shi, and D. Bruley, Eds. Cham: Springer, 2016, vol. 923, Advances in Experimental Medicine and Biology. [Online]. Available: https://doi.org/10.1007/978-3-319-38810-6_26

34. Wang, X., Tian, F., Soni, S. S., Gonzalez-Lima, F., & Liu, H. (2016). Interplay between up- regulation of cytochrome-c-oxidase and hemoglobin oxygenation induced by near-infrared laser. _Scientific reports_, _6_(1), 1-10

35. T. V. Vo, P. E. Hammer, M. L. Hoimes, S. Nadgir, and S. Fantini, "Mathematical Model for the Hemodynamic Response to Venous Occlusion Measured With Near-Infrared Spectroscopy in the Human Forearm," in IEEE Transactions on Biomedical Engineering, vol. 54, no. 4, pp. 573-584, Apr. 2007. [Online]. Available: https://doi.org/10.1109/TBME.2006.890123

36. P. Léné et al., "Wavelet Transform Coherence: An Innovative Method to Investigate Social Interaction in NeuroIS," in Information Systems and Neuroscience, F. Davis, R. Riedl, J. vom Brocke, P. M. Léger, A. Randolph, and T. Fischer, Eds. Cham: Springer,

2020, vol. 32, Lecture Notes in Information Systems and Organisation. [Online]. Available: https://doi.org/10.1007/978-3-030-28144-1_16

37. Kvernmo, H. D., A. Stefanovska, K. A. Kirkeboen, and K. Kvernebo. 1999. 'Oscillations in the human cutaneous blood perfusion signal modified by endothelium-dependent and endothelium-independent vasodilators', Microvasc Res, 57: 298-309.

38. Bastos AM, Schoffelen JM. A Tutorial Review of Functional Connectivity Analysis Methods and Their Interpretational Pitfalls. Front Syst Neurosci. 2016 Jan 8;9:175. doi: 10.3389/fnsys.2015.00175. PMID: 26778976; PMCID: PMC4705224.

39. Z. T. Martin, J. D. Akins, E. R. Merlau, J. O. Kolade, I. O. Al-daas, N. Cardenas, J. K. Vu, K. K. Brown, and R. M. Brothers, "The acute effect of whole-body heat therapy on peripheral and cerebral vascular reactivity in Black and White females," Microvascular Research, vol. 148, 2023. [Online]. Available: [https://doi.org/10.1016/j.mvr.2023.104536].

40. "Effects of Race and Hypertension on Flow-Mediated and Nitroglycerin-Mediated Dilation of the Brachial Artery," American Heart Association Journals, 2023. [Online]. Available: https://www.ahajournals.org/doi/pdf/10.1161/hy1201.096575.

41. J. D. Akins, Z. T. Martin, J. C. Patik, B. M. Curtis, J. C. Campbell, G. Olvera, and R. M. Brothers, "Young, non-Hispanic Black men and women exhibit divergent peripheral and cerebral vascular reactivity," The Physiological Society, 2022. [Online]. Available: [https://doi.org/10.1113/EP090168].

42. D. J. Hausenloy and D. M. Yellon, "The Second Window of Preconditioning (SWOP) Where Are We Now?," Cardiovasc Drugs Ther, vol. 24, pp. 235-254, 2010. [Online]. Available: https://doi.org/10.1007/s10557-010-6237-9

43. Multi-Taper Method (MTM)," UCLA Department of Atmospheric and Oceanic Sciences, 2023. [Online]. Available: https://dept.atmos.ucla.edu/tcd/multi-taper-method-mtm. [Accessed: Apr. 4, 2023].

44. Slepian or DPSS Window, CCRMA, Stanford University, 2023. [Online]. Available: https://ccrma.stanford.edu/~jos/sasp/Slepian_DPSS_Window.html. [Accessed: Apr. 4, 2023].

45. Dezfulian C, Garrett M, Gonzalez NR. Clinical application of preconditioning and postconditioning to achieve neuroprotection. Transl Stroke Res. 2013 Feb;4(1):19-24. doi: 10.1007/s12975-012-0224-3. Epub 2012 Nov 15. PMID: 24323188; PMCID: PMC4224593.

46. Wang A, Brothers RM, Hurr C. Application of blood flow restriction in hypoxic environment augments muscle deoxygenation without compromising repeated sprint exercise performance. Exp Physiol. 2023 Mar 19. doi: 10.1113/EP091032. Epub ahead of print. PMID: 36934386.

47. S. Baig, B. Moyle, K. P. S. Nair, et al., "Remote ischaemic conditioning for stroke: unanswered questions and future directions," Stroke and Vascular Neurology, vol. 6, 2021. [Online]. Available: https://doi.org/10.1136/svn-2020-000722

48. Das DK, Engelman RM, Rousou JA, Breyer RH. Aerobic vs anaerobic metabolism during ischemia in heart muscle. Ann Chir Gynaecol. 1987;76(1):68-76. PMID: 3592561.

49. Lalonde, François; Curnier, Daniel Y. Can Anaerobic Performance Be Improved by Remote Ischemic Preconditioning?. Journal of Strength and Conditioning Research 29(1):p 80-85, January 2015. | DOI: 10.1519/JSC.0000000000000609
50. All illustrations were created with BioRender.com